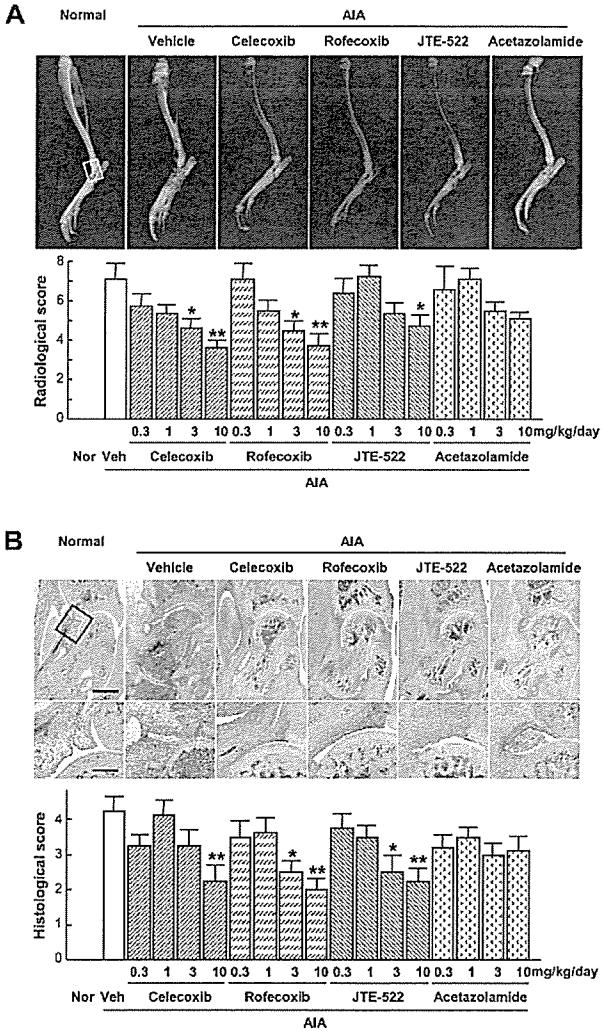


**FIG. 5.** Inhibitory effects of COX-2 and CA II–selective agents on joint destruction in AIA rats. (A) Representative radiographs of right hindlimbs of normal and AIA rats with and without application of celecoxib, rofecoxib, JTE-522, and acetazolamide. The graph shows the dose response of inhibitory effects of the agents on radiological scoring. A 0–5 grading system (0 = normal, 5 = the most severe) was used to evaluate bone destruction and periostitis, respectively, and the sum of the scores for the parameters was calculated (maximum 10). (B) Representative histological features (H&E staining) with low (upper) and high (lower) magnifications of the talo-tibial joints of normal and AIA rats with and without application of celecoxib, rofecoxib, JTE-522, and acetazolamide. The inset box in A indicates the region of the upper figure in B, and that in the upper figure indicates the region of the lower figure. Bar, 200 and 50 μm. The graph shows the dose response of inhibitory effects of the agents on histological scoring. A 0–5 subjective grading system (0 = normal, 5 = the most severe) was used to evaluate the overall change including synovial thickening (pannus formation) and joint destruction (maximum 5). Data are expressed as means (bars) ± SE (error bars) for eight animals per group. $*p < 0.05$, $**p < 0.01$; significant inhibition by the agents.

biological therapies targeting these cytokines are known to be the most effective treatment for RA bone destruction.[30] Regarding the cytokines used in the in vitro studies, FGF-2 stimulates both differentiation and activity of osteoclasts and has been reported to play a role in RA bone destruction in the animal model and clinical settings.[2–4] On the other hand, Gas6 that stimulates only osteoclast activity is reported to be involved in bone loss by estrogen deficiency but not in RA bone destruction.[17] In addition to the differentiation and activity of osteoclasts, their survival might be another therapeutic target for RA bone destruction. Although these studies showed that none of the COX-2 selective agents or acetazolamide affected the survival of mature osteoclasts generated and isolated from the M-BMMϕ culture (data not shown), bisphosphonates that inhibit the osteoclast survival are now considered to be a possible candidate to treat this disorder.[31,32]

In this study, the same range of dosage (0.3–10 mg/kg/day) was applied to AIA rats for all drugs, which were decided according to previous reports on their anti-inflammatory potencies in the same model.[33–35] This range of dosage was also determined to cover their clinical daily dosages: 4 mg/kg for celecoxib, 0.5 mg/kg for rofecoxib, 2–5 mg/kg for JTE-522, and 5 mg/kg for acetazolamide. Although the dosage of rofecoxib seems about 1/10 of those of other drugs, gastrointestinal absorption of this drug in rats is reported to be about 1/10 that in humans,[36,37] suggesting that these drugs of the same dosage have similar biological potencies in AIA rats. Indeed, this does not lead to the conclusion that the efficacy of the agents can be compared simply by the $ED_{50}$ values calculated by the dose-response experiments (Fig. 4); however, the fact that the $ED_{50}$ value of JTE-522 with the strongest potency of CA II inhibition (Fig. 2) was higher than other COX-2 inhibitors also implies that CA II inhibition is less important than COX-2 inhibition for the suppression of AIA bone destruction.

The representative COX-2 selective agents celecoxib and rofecoxib have been reported to yield similar efficacy comparable with conventional nonsteroidal anti-inflammatory drugs (NSAIDs) with less incidence of gastrointestinal side effects.[38–40] This study, however, revealed a discrepancy of their biological effects: celecoxib inhibited mature osteoclast activity, whereas rofecoxib did not. This may be because of the sulfonamide moiety that has the potency to inhibit CA II, because JTE-522 and acetazolamide with the moiety also inhibited the mature osteoclast activity, whereas SC-560 without it[24] did not. Recent studies also have provided evidence that the use of celecoxib and rofecoxib can lead to several differences in response patterns in animal models as well as in the clinic.[40] In glaucomatous rabbits, celecoxib, but not rofecoxib, lowered intraocular pressure similarly to acetazolamide, a conventional drug for glaucoma.[24] The sulfonamides are known to constitute an important class of drugs possessing not only anticarbonic anhydrase, but also antibacterial, diuretic, hypoglycemic, antithyroid, protease inhibitory, and anticancer activities,[41] suggesting that the sulfonamide-type COX-2 inhibitors such as celecoxib and JTE-522 may have use in the treatment of these disorders. More importantly, a recent social topic is that rofecoxib significantly increased the risk of cardiovascular events in clinical trials, which finally led to the voluntary worldwide withdrawal of this drug, although

it is controversial whether this serious adverse event is common to COX-2 selective agents including celecoxib or, more generally, to NSAIDs.[42,43]

This study used mouse cell cultures and a rat arthritic model for in vitro and in vivo analyses, respectively, and suggested the significant effect of COX-2 selective agents not only on inflammation but also on arthritic bone resorption. Accumulated evidence has also shown the bone-sparing effects of COX-2 inhibitors using mouse and rat models in vitro and in vivo.[10,34,44–47] Because both COX-2 and CAII show 80–90% homologies in nucleotides and amino acids among mice, rats, and humans,[48–50] these results may be applicable to humans. For the clinical application of COX-2 selective agents as a treatment of bone resorptive disorders including RA, however, we should be cautious not only with cardiovascular events above, but also with possible inhibition of bone repair and ingrowth that has recently been reported in animal models when administered for a long period of time.[51–53] A large-scale clinical trial will clarify the possibility and limitation of these drugs as a novel treatment of the skeletal disorders.

## ACKNOWLEDGMENTS

The authors thank Reiko Yamaguchi and Miki Koshimizu at University of Tokyo for technical assistance. This study was supported by Grants-in-Aid for Scientific Research from the Japanese Ministry of Education, Science, Sports, Culture and Technology (10470302 and 16659402).

## REFERENCES

1. Shimizu S, Shiozawa S, Shiozawa K, Imura S, Fujita T 1985 Quantitative histologic studies on the pathogenesis of periarticular osteoporosis in rheumatoid arthritis. Arthritis Rheum **28:**25–31.
2. Manabe N, Oda H, Nakamura K, Kuga Y, Uchida S, Kawaguchi H 1999 Involvement of fibroblast growth factor-2 in joint destruction of rheumatoid arthritis patients. Rheumatol **38:**714–720.
3. Nakano K, Okada Y, Saito K, Tanaka Y 2004 Induction of RANKL expression and osteoclast maturation by the binding of fibroblast growth factor 2 to heparan sulfate proteoglycan on rheumatoid synovial fibroblasts. Arthritis Rheum **50:**2450–2458.
4. Yamashita A, Yonemitsu Y, Okano S, Nakagawa K, Nakashima Y, Irisa T, Iwamoto Y, Nagai Y, Hasegawa M, Sueishi K 2002 Fibroblast growth factor-2 determines severity of joint disease in adjuvant-induced arthritis in rats. J Immunol **168:**450–457.
5. Kawaguchi H, Pilbeam CC, Harrison JR, Raisz LG 1995 The role of prostaglandins in the regulation of bone metabolism. Clin Orthop **313:**36–46.
6. Suda T, Takahashi N, Udagawa N, Jimi E, Gillespie MT, Martin TJ 1999 Modulation of osteoclast differentiation and function by the new members of the tumor necrosis factor receptor and ligand families. Endocr Rev **20:**345–357.
7. Fuller K, Chambers TJ 1989 Effect of arachidonic acid metabolites on bone resorption by isolated rat osteoclasts. J Bone Miner Res **4:**209–215.
8. Kawaguchi H, Pilbeam CC, Gronowicz G, Abreu C, Fletcher BS, Herschman HR, Raisz LG, Hurley MM 1995 Transcriptional induction of prostaglandin G/H synthase-2 by basic fibloblast growth factor. J Clin Invest **96:**923–930.
9. Kawaguchi H, Nemoto K, Raisz LG, Harrison JR, Voznesensky OS, Alander CB, Pilbeam CC 1994 Interleukin-4 inhibits prostaglandin G/H synthase-2 and cytosolic phospholipase A2 induction in neonatal mouse parietal bone cultures. J Bone Miner Res **11:**358–366.
10. Kawaguchi H, Chikazu D, Nakamura K, Kumegawa M, Hakeda Y 2000 Direct and indirect actions of fibroblast growth factor 2 on osteoclastic bone resorption in cultures. J Bone Miner Res **15:**466–473.
11. Chikazu D, Katagiri M, Ogasawara T, Ogata N, Shimoaka T, Takato T, Nakamura K, Kawaguchi H 2001 Regulation of osteoclast differentiation by fibroblast growth factor 2: Stimulation of receptor activator of nuclear factor kappaB ligand/osteoclast differentiation factor expression in osteoblasts and inhibition of macrophage colony-stimulating factor function in osteoclast precursors. J Bone Miner Res **16:**2074–2081.
12. Okada Y, Lorenzo JA, Freeman AM, Tomita M, Morham SG, Raisz LG, Pilbeam CC 2000 Prostaglandin G/H synthase-2 is required for maximal formation of osteoclast-like cells in culture. J Clin Invest **105:**823–832.
13. Kawaguchi H, Pilbeam CC, Vargas SJ, Morse EE, Lorenzo JA, Raisz LG 1995 Ovariectomy enhances and estrogen replacement inhibits the activity of bone marrow factors that stimulate prostaglandin production in cultured mouse calvariae. J Clin Invest **96:**539–548.
14. Schuna AA, Megeff C 2000 New drugs for the treatment of rheumatoid arthritis. Am J Health Syst Pharm **57:**225–234.
15. Nakamura YS, Hakeda Y, Takekura N, Kameda T, Hamaguchi I, Miyamoto T, Kakudo S, Nakano T, Kumegawa M, Suda T 1998 Tyro 3 receptor tyrosine kinase and its ligand, Gas6, stimulate the function of osteoclasts. Stem Cells **18:**229–238.
16. Chikazu D, Hakeda Y, Ogata N, Nemoto K, Itabashi A, Takato T, Kumegawa M, Nakamura K, Kawaguchi H 2000 Fibroblast growth factor (FGF)-2 directly stimulates mature osteoclast function through activation of FGF receptor 1 and p42/p44 MAP kinase. J Biol Chem **275:**31444–31450.
17. Katagiri M, Hakeda Y, Chikazu D, Ogasawara T, Takato T, Kumegawa M, Nakamura K, Kawaguchi H 2001 Mechanism of stimulation of osteoclastic bone resorption through Gas6/Tyro 3, a receptor tyrosine kinase signaling, in mouse osteoclasts. J Biol Chem **276:**7376–7382.
18. Bekker PJ, Gay CV 1990 Biochemical characterization of an electrogenic vacuolar proton pump in purified chicken osteoclast plasma membrane vesicles. J Bone Miner Res **6:**569–579.
19. Rousselle AV, Heymann D 2002 Osteoclastic acidification pathways during bone resorption. Bone **30:**533–540.
20. Teti A, Blair HC, Teitelbaum SL, Kahn AJ, Koziol C, Konsek J, Zambonin-Zallone A, Schlesinger PH 1989 Cytoplasmic pH regulation and chloride/bicarbonate exchange in avian osteoclasts. J Clin Invest **83:**227–233.
21. Laitala T, Vänänen HK 1994 Inhibition of bone resorption *in vitro* by antisense RNA and DNA molecules targeted against carbonic anhydrase II or two subunits of vacuolar $H^+$-ATPase. J Clin Invest **93:**2311–2318.
22. Sly WS, Hu PY 1995 Human carbonic anhydrases and carbonic anhydrase deficiencies. Annu Rev Biochem **64:**375–401.
23. Asotra S, Gupta AK, Sodek J, Aubin JE, Heershe JNM 1995 Carbonic anhydrase II mRNA expression in individual osteoclasts under "resorbing" and "nonresorbing" conditions. J Bone Miner Res **9:**1115–1122.
24. Weber A, Casini A, Heine A, Kuhn D, Supuran CT, Scozzafava A, Klebe G 2004 Unexpected nanomolar inhibition of carbonic anhydrase by COX-2-Selective celecoxib: New pharmacological opportunities due to related binding site recognition. J Med Chem **47:**550–557.
25. Zimmermann M 1983 Ethical guidelines for investigations of experimental pain in conscious animals. Pain **16:**109–110.
26. Matsushita M, Masaki M, Yagi Y, Tanaka T, Wakitani K 1997 Pharmacological profile of JTE-522, a novel prostaglandin H synthase-2 inhibitor, in rats. Inflamm Res **46:**461–466.
27. Kobayashi K, Takahashi N, Jimi E, Udagawa N, Takami M, Kotake S, Nakagawa N, Kinosaki M, Yamaguchi K, Shima N, Yasuda H, Morinaga T, Higashio K, Martin TJ, Suda T 2000 Tumor necrosis factor alpha stimulates osteoclast differentia-

tion by a mechanism independent of the ODF/RANKL-RANK interaction. J Exp Med **191:**275–286.
28. Wilbur KM, Anderson NG 1948 Electrometric and colorlimetric determination of carbonic anhydrase. J Biol Chem **176:**147–154.
29. Suda T, Kobayashi K, Jimi E, Udagawa N, Takahashi N 2001 The molecular basis of osteoclast differentiation and activation. Novartis Found Symp **232:**235–247.
30. Olsen NJ, Stein CM 2004 New drugs for rheumatoid arthritis. N Engl J Med **350:**2167–2179.
31. Herrak P, Gortz B, Hayer S, Redlich K, Reiter E, Gasser J, Bergmeister H, Kollias G, Smolen JS, Schett G 2004 Zoledronic acid protects against local and systemic bone loss in tumor necrosis factor-mediated arthritis. Arthritis Rheum **50:**2327–2337.
32. Sims NA, Green JR, Glatt M, Schlict S, Martin TJ, Gillespie MT, Romas E 2004 Targeting osteoclasts with zoledronic acid prevents bone destruction in collagen-induced arthritis. Arthritis Rheum **50:**2338–2346.
33. Chan CC, Boyce S, Brideau C, Charleson S, Cromlish W, Ethier D, Evans J, Ford-Hutchinson AW, Forrest MJ, Gauthier JY, Gordon R, Gresser M, Guay J, Kargman S, Kennedy B, Leblanc Y, Leger S, Mancini J, O'Neill GP, Ouellet M, Patrick D, Percival MD, Perrier H, Prasit P, Rodger I 1999 Rofecoxib [Vioxx, MK-0966; 4-(4′-Methylsulfonylphenyl)-3-phenyl-2-(5H)-furanone]: A potent and orally active cyclooxygenase-2 inhibitor. Pharmacological and biochemical profiles. J Pharmacol Exp Ther **290:**551–560.
34. Masaki M, Matsushita M, Wakitani K 1998 Inhibitory effects of JTE-522, a novel prostaglandin H synthase-2 inhibitor, on adjuvant-induced arthritis and bone changes in rats. Inflamm Res **47:**187–192.
35. Nolan JC, Gathright CE, Radvany CH, Barrett RJ, Sancilio LF 1991 Carbonic anhydrase inhibitors are antiarthritic in the rat. Pharmacol Res **24:**377–383.
36. Mandal U, Ganesan M, Jayakumar M, Pal TK, Chattaraj TK, Ray K, Banerjee SN 2003 High performance liquid chromatographic determination of Cox-2 inhibitor rofecoxib in human plasma. J Indian Med Assoc **101:**486–488.
37. Halpin RA, Porras AG, Geer LA, Davis MR, Cui D, Doss GA, Woolf E, Musson D, Matthews C, Mazenko R, Schwartz JI, Lasseter KC, Vyas KP, Baillie TA 2002 The disposition and metabolism of rofecoxib, a potent and selective cyclooxygenase-2 inhibitor, in human subjects. Drug Metab Dispos **30:**684–693.
38. Bombardier C, Laine L, Reicin A, Shapiro D, Burgos-Vargas R, Davis B, Day R, Ferraz MB, Hawkey CJ, Hochberg MC, Kvien TK, Schnitzer TJ, Study Group VIGOR 2000 Comparison of upper gastrointestinal toxicity of rofecoxib and naproxen in patients with rheumatoid arthritis. N Engl J Med **343:**1520–1528.
39. Silverstein FE, Faich G, Goldstein JL, Simon LS, Pincus T, Whelton A, Makuch R, Eisen G, Agrawal NM, Stenson WF, Burr AM, Zhao WW, Kent JD, Lefkowith JB, Verburg KM, Geis GS 2000 Gastrointestinal toxicity with celecoxib vs. nonsteroidal anti-inflammatory drugs for osteoarthritis and rheumatoid arthritis: The CLASS study: A randomized controlled trial. Celecoxib Long-term Arthritis Safety Study. JAMA **284:**1247–1255.
40. FitzGerald GA, Patrono C 2001 The coxibs, selective inhibitors of cyclooxygenase-2. N Engl J Med **345:**433–442.
41. Supuran CT, Casini A, Mastrolorenzo A, Scozzafava A 2004 Cox-2 selective inhibitors, carbonic anhydrase inhibition and anticancer propaties of sulfonamides belonging to this class of pharmacological agents. Mini Rev Med Chem **4:**625–632.
42. Jüni P, Dieppe P 2004 Older people should NOT be prescribed "coxibs" in place of conventional NSAIDs. Age Ageing **33:**100–104.
43. Dieppe PA, Ebrahim S, Martin RM, Juni P 2004 Lessons from the withdrawal of rofecoxib. BMJ **329:**867–868.
44. Inoue K, Motonaga A, Suzuka H, Yoshifusa H, Fujisawa H, Nishimura T, Inoue Y, Ueda F, Shibata Y, Kimura K 1993 Effect of etodolac on type-II collagen-induced arthritis in mice. Agents Actions **39:**187–194.
45. Weichman BM, Chau TT, Rona G 1987 Histopathologic evaluation of the effects of etodolac in established adjuvant arthritis in rats: Evidence for reversal of joint damage. Arthritis Rheum **30:**466–470.
46. Engelhardt G, Homma D, Schnitzler C 1995 Meloxicam: A potent inhibitor of adjuvant arthritis in the Lewis rat. Inflamm Res **44:**548–555.
47. Igarashi K, Woo JT, Stern PH 2002 Effects of a selective cyclooxygenase-2 inhibitor, celecoxib, on bone resorption and osteoclastogenesis *in vitro.* Biochem Pharmacol **63:**523–532.
48. Venta PJ, Montgomery JC, Hewett-Emmett D, Wiebauer K, Tashian RE 1985 Structure and exon to protein domain relationships of the mouse carbonic anhydrase II gene. J Biol Chem **260:**12130–12135.
49. Murakami H, Marelich GP, Grubb JH, Kyle JW, Sly WS 1987 Cloning, expression, and sequence homologies of cDNA for human carbonic anhydrase II. Genomics **1:**159–166.
50. Song JH, Sirois J, Houde A, Murphy BD 1998 Cloning, developmental expression, and immunohistochemistry of cyclooxygenase 2 in the endometrium during embryo implantation and gestation in the mink. Endocrinology **139:**3629–3636.
51. Gerstenfeld LC, Einhorn TA 2004 COX inhibitors and their effects on bone healing. Expert Opin Drug Saf **3:**131–136.
52. Goodman S, Ma T, Trindade M, Ikenoue T, Matsuura I, Wong N, Fox N, Genovese M, Regula D, Smith RL 2002 COX-2 selective NSAID decreases bone ingrowth *in vivo.* J Orthop Res **20:**1164–1169.
53. Goodman SB, Ma T, Mitsunaga L, Miyanishi K, Genovese MC, Smith RL 2005 Temporal effects of a COX-2-selective NSAID on bone ingrowth. J Biomed Mater Res A **72:**279–287.

Address reprint requests to:
*Hiroshi Kawaguchi, MD, PhD*
*Sensory & Motor System Medicine*
*Faculty of Medicine*
*University of Tokyo*
*Hongo 7-3-1, Bunkyo*
*Tokyo 113-8655, Japan*
*E-mail: kawaguchi-ort@h.u-tokyo.ac.jp*

Received in original form April 8, 2005; revised form August 15, 2005; accepted October 31, 2005.

# Isolation of Murine Hair-Inducing Cells Using the Cell Surface Marker Prominin-1/CD133

Yuriko Ito[1], Tatsuo S Hamazaki[1,2,3], Kiyoshi Ohnuma[2], Kunihiko Tamaki[4], Makoto Asashima[2,3] and Hitoshi Okochi[1]

Hair is a mini-organ in which dermal papilla (DP) cells play important roles in hair follicle morphogenesis and formation via interactions with epithelial cells. DP cells have previously been difficult to analyze because of the lack of a specific surface marker. We have demonstrated that prominin-1/CD133 (CD133) is a useful marker for murine DP cells. DP cells express CD133 during the early anagen stage (active growth phase) not only during hair morphogenesis, but also during the growth phase of hairs after birth. Gene expression and flow cytometric analysis revealed that CD133-positive (+) cells in the skin possess the characteristics of DP cells. The CD133(+) cells isolated from embryonic or adult skin-induced new hair follicles *in vivo* when they were transplanted into nude mice mixed with embryonic epithelial cells, but CD133-negative(−) cells could not. We propose that the CD133 is a novel surface marker useful for collecting DP cells in the anagen stage and for analyzing the function of DP.

*Journal of Investigative Dermatology* advance online publication, 21 December 2006; doi:10.1038/sj.jid.5700665

## INTRODUCTION

Hair undergoes recurring growth cycles throughout life. Two major components, follicular epithelium and dermal papilla (DP), develop and remodel hair follicles by reciprocal communication (Schmidt-Ullrich and Paus, 2005). DP cells are considered essential to hair follicle induction because transplantation of DP cells beneath the epithelium induces *de novo* hair growth in hairless skin such as palms and soles (Reynolds and Jahoda, 1992). The hair follicle inducing cells in DP are referred to as dermal mesenchyme/fibroblasts based upon their morphological characteristics (Paus *et al.*, 1999; Paus and Foitzik, 2004). It has been difficult to isolate dermal mesenchyme/fibroblasts without reliable and specific surface markers. DP cells can be harvested by excision of rodent vibrissae and human scalp hair follicles. However, because their structure is so minute, it is difficult to isolate DP cells from the pelage hairs of embryonic and adult skin. Prior studies have indicated that DP cells produce adhesion molecules, enzymes, growth modulators, growth factors, proteoglycans, and receptors (see table by Botchkarev and Kishimoto, 2003). However, these receptors are not suitable for isolating DP cells, because other cell types in the skin also express them. Among the proteoglycans, versican was evaluated for its relationship to the hair follicle-inducing ability of DP cells (Kishimoto *et al.*, 1999). As the green fluorescence protein (GFP)-positive cells of versican-GFP transgenic mice succeeded in inducing hair growth, hair follicle-inducing cells could be isolated from the gene-manipulated animals.

In our search for a specific marker for isolating DP cells from non-transgenic mice, we selected a membranous protein, CD133, as a candidate. CD133 was first described as a marker for human hematopoietic stem cells (Yin *et al.*, 1997) and has recently been proposed as a universal marker for tissue stem/progenitor cells (Weigmann *et al.*, 1997; Uchida *et al.*, 2000; Richardson *et al.*, 2004; Bussolati *et al.*, 2005). In this study, we determined that DP cells express CD133. Moreover, we were able to isolate CD133-positive (+) cells and show that they possess hair follicle-inducing capability.

## RESULTS

### Stage-specific expression of CD133 on dermal condensate/papilla cells during hair follicle development and the hair cycle after birth

We first stained samples of embryonic dorsal skin (E18.5) with anti-CD133 antibody. The expression of CD133 was observed mainly on dermal condensate/papilla cells and a few cells in the dermal sheath (Figure 1a and b). No other cells in the epidermis, dermis, or fat tissue expressed the marker. To examine when the DP cells produce CD133, we obtained skin specimens from embryos at various stages and neonates. In the dorsal skin, DP cells expressed CD133 primarily from embryonic developmental day 16.5 (E16.5)

[1]*Department of Tissue Regeneration, Research Institute, International Medical Center of Japan, Toyama, Shinjuku, Tokyo, Japan;* [2]*Department of Life Science, Graduate School of Art and Sciences, The University of Tokyo, Komaba, Meguro, Tokyo, Japan;* [3]*International Cooperative Research Project (ICORP) of JST, Tokyo, Japan;* [4]*Department of Dermatology, Faculty of Medicine, The University of Tokyo, Hongo, Bunkyo, Tokyo, Japan*

*Correspondence: Dr Hitoshi Okochi, Department of Tissue Regeneration, Research Institute, International Medical Center of Japan, Toyama 1-21-1, Shinjuku, Tokyo 162-8655, Japan. E-mail: hokochi@ri.imcj.go.jp*

*Abbreviations: GFP, green fluorescence protein; PBS, phosphate-buffered saline; p75NTR, p75 neutrophin receptor; SKP, skin-derived precursor*

*Received 8 June 2006; revised 2 October 2006; accepted 2 October 2006*

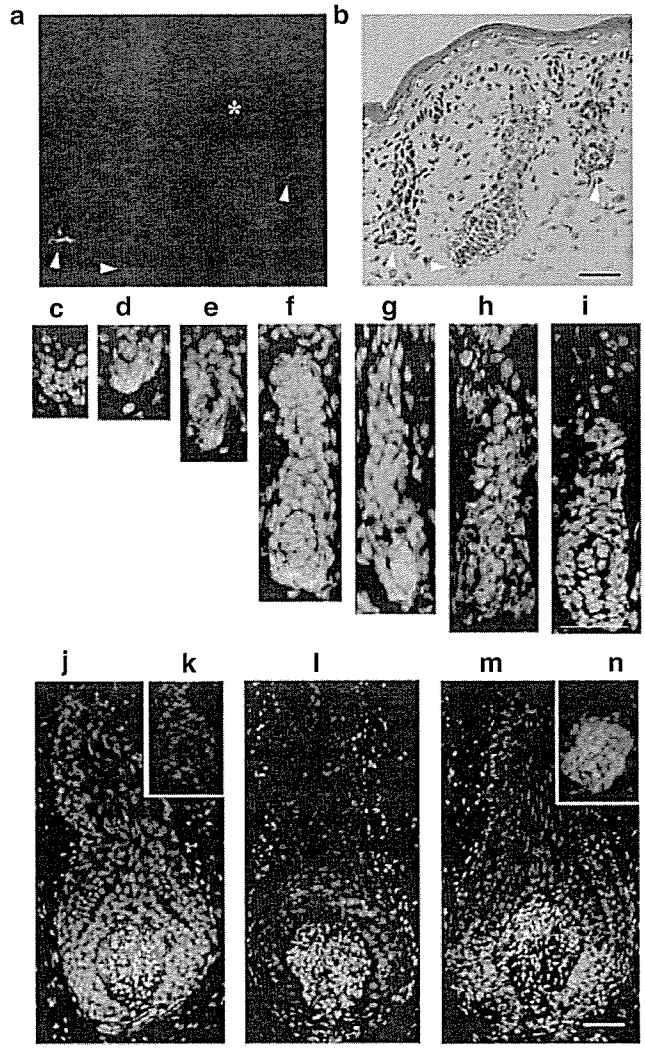


**Figure 1. DP cells express CD133 during the early anagen stage.** Low magnification view of the dermis of E18.5 mice stained with the (**a**) anti-CD133 antibody and counterstained with (**b**) hematoxylin-eosin. The expression of CD133 was observed mainly in the DP cells (arrowhead) but other parts, including the bulge area (asterisk) did not. (**c–i**) Dermal condensate and papilla cells were positive for CD133 during hair morphogenesis. Although the CD133 is a membranous protein, positive cytoplasmic staining was observed because the bound anti-CD133 antibody was enhanced with tyramide. The dorsal skin of E17.5, E18.5 and P0, P1, P2 mice stained with the anti-CD133 antibody and CD133 (+) cells was visualized with red fluorescence. Nuclei were stained blue using Hoechst dye. (**c**) stage 1, (**d**) stage 2, (**e**) stage 3, (**f**) stage 4, (**g**) stage 5, (**h**) stages 5–6, (**i**) stage 7 anagen. CD133 expression in the DP was detected from stages 2–5 anagen of hair development. (**j–n**) The CD133 protein reappeared on DP cells during second anagen and also during induced anagen of adult hairs. The DP in (**j**) early second-anagen vibrissae and (**k**) pelage hairs of 4-week-old mice expressed CD133, but the DP in (**l**) mid-anagen of 7-week-old mice did not. Both (**m**) vibrissae and (**n**) pelage hairs plucked from 7-week-old mice to artificially induce early anagen showed CD133 expression. All bars represent 100 $\mu$m.

until postnatal day 1 (P1; second day of life). The developmental stages of hair growth are histologically categorized from stages 1 to 8 (Paus *et al.*, 1999). The stage of each hair follicle was determined morphologically, according to this classification. Immunohistochemical analysis revealed that

**Table 1. Rate of CD133 (+) cells in the skin**

| Developmental age | CD133 (+) cells percentage ± SD |
|---|---|
| E16.5 | 4.40 ± 0.10 ($n$=10) |
| E17.5 | 2.17 ± 0.18 ($n$=15)*** |
| E18.5 | 1.60 ± 0.03 ($n$=10)*** |
| P1 | 0.69 ± 0.03 ($n$=5)*** |
| P5 | 0.26 ± 0.04 ($n$=3)*** |
| 8W | 0.38 ± 0.03 ($n$=3) |
| 8W[1] | 2.10 ± 0.11 ($n$=3)(***) |

E, embryonic developmental day; P, postnatal day; W, weeks after birth. Specimens were obtained from the back skin of embryos/neonates and scalp skin of adults.
The percentage of CD133 (+) cells in E16.5 was compared with those of E17.5, E18.5, P1, and P5. Statistical significance was determined by Student's $t$-test.
***$P<0.001$.
(***)Significant difference ($P<0.001$) of the percentage between depilated and untreated skin in adult mice.
[1]Mice were used 6 days after depilation when newly induced hairs were at the anagen stage. In each sample, $1 \times 10^6$ dissociated cells were incorporated, and the number of CD133 (+) cells was counted by the flowcytometer.

the expression of CD133 on dermal condensate/papilla cells was detected during stages 2–5 (Figure 1d–g) of hair morphogenesis. Particularly, strong expression of this molecule was observed in stages 3 and 4 (Figure 1e and f). A few cells in the dermal sheath expressed CD133 from stages 4 to 5. To calculate the percentage of CD133 (+) cells in back skin, samples containing $1 \times 10^6$ dermal cells of various age groups were analyzed, and positively stained cells were counted by the flow cytometer. As shown in Table 1, the percentage of CD133 (+) cells was 4.4% at E16.5, gradually declined until birth, and then rapidly decreased to 0.3% after birth. To certify whether CD133 (+) cells reappear in the DP after birth, we collected skin specimens from 3- to 4-week-old mice when the hair cycle synchronizes and enters the next cycle, the second anagen phase (Muller-Rover *et al.*, 2001). Immunohistochemical staining showed that DP of vibrissae and pelage hairs transiently express CD133 during the secondary early anagen (Figure 1k). In the adult, hairs follow independent hair cycles, but if the hairs are artificially plucked, their random hair stages synchronize to enter into new hair cycles. The anagen phase of the hair cycle was induced in 7-week-old mice by plucking their vibrissae and pelage hairs under anesthesia. Six days after depilation, when the stage of the hair cycle advances from telogen to early anagen, the DP cells transiently expressed CD133 (Figure 1m and n). CD133 (+) cells were observed in the DP at 6, 7, and 8 days after depilation. The percentage of CD133 (+) cells in adult skin increased from 0.4 to 2% after depilation (Table 1). In this study, a monoclonal antibody, clone 13A4, was mainly used for immunostaining. The positive expression of CD133 on DP cells was confirmed by another primary antibody, raised in a rabbit (data not shown). Unfortunately, we could not detect similar staining pattern for CD133 in human DP cells (data not shown).

**DP cells express CD133 before the production of versican**

Versican is one of the extracellular matrices produced by DP cells (du Cros *et al.*, 1995). Moreover, the versican producing cells were reported to induce hair follicles *in vivo* in implantation experiments (Kishimoto *et al.*, 1999). To evaluate whether the CD133 (+) cells of DP co-express versican, we double-stained skin specimens of embryonic and adult mice with anti-CD133 and anti-versican antibodies. The immunohistological analysis showed that the expression of CD133 preceded the production of versican (Figure 2a–d) during the hair development, but the positivity for versican continued after the CD133 expression was no longer detected (Figure 2e). During the second anagen phase after birth, the DP cells transiently co-expressed the two proteins (Figure 2f and g). The DP cells stained positively for versican but not for CD133 during the late-anagen stage (Figure 2h).

Isolated CD133 (+) cells of the skin were cultured to verify whether they started to produce versican, *in vitro*. CD133 (+) cells from E16.5 skin (Figure 2i) were initially negative for versican (Figure 2j); however, after cultivation for 3 days, they began to proliferate and produce versican (Figure 2m), as they stopped producing CD133 (Figure 2l). Versican-positive cells (Figure 2k) maintained versican expression after proliferation (Figure 2n).

**Phenotypical analysis of CD133 (+) cells**

Immunocytometric analysis by flow cytometry revealed that CD133 (+) cells of embryonic skin, E16.5, were also positive for CD44 (Tuhkanen *et al.*, 1999), CD56/neural cell adhesion molecule (Muller-Rover *et al.*, 1998), p75 neutrophin receptor (p75NTR) (Botchkareva *et al.*, 1999), nestin, and CD90/Thy-1, but they were negative for Sca-1, CD117/c-kit, CD45, CD202/Tie-2, and desmoglein (Figure 3). These results suggest that CD133 (+) cells do not include any hematopoetic, melanocytic, endothelial, or epithelial cells.

**Analysis of gene expression in CD133 (+) cells**

To confirm that the isolated CD133 (+) cells transcribe several genes, which DP cells have been reported to express, we analyzed their gene expression by quantitative PCR. Total RNA was extracted from CD133 (+) cells isolated from the skin of E16.5 embryos, and of 8-week-old mice whose hairs had been plucked 6 days previously. The results of real-time PCR showed that in E16.5, CD133 (+) cells expressed *CD133*, *twist1*, *slug1*, *hey1*, *INHBA*, *BMP4*, *wise*, *nexin1*, *PDGFRa*, and *FGF7* twice as strongly as CD133-negative (−) cells (Figure 4a). In adult CD133 (+) cells, *twist1*, *slug1*, *snail1*, *hey1*, *INHBA*, *BMP4*, *versican*, *nexin1*, *PDGFRa*, *IGFBP3*, and *FGF7* were the genes that were twice as strongly expressed in CD133 (−) cells (Figure 4b). A prior study of microarrays had already shown that DP cells of P4 expressed these genes (Rendl *et al.*, 2005).

When PCR reactions were performed with templates from CD133 (+) cells of embryonic and adult skin, only one PCR product of 205 bp was amplified (data not shown). The band corresponded to a splicing variant, prominin-1.s1 (Fargeas *et al.*, 2004).

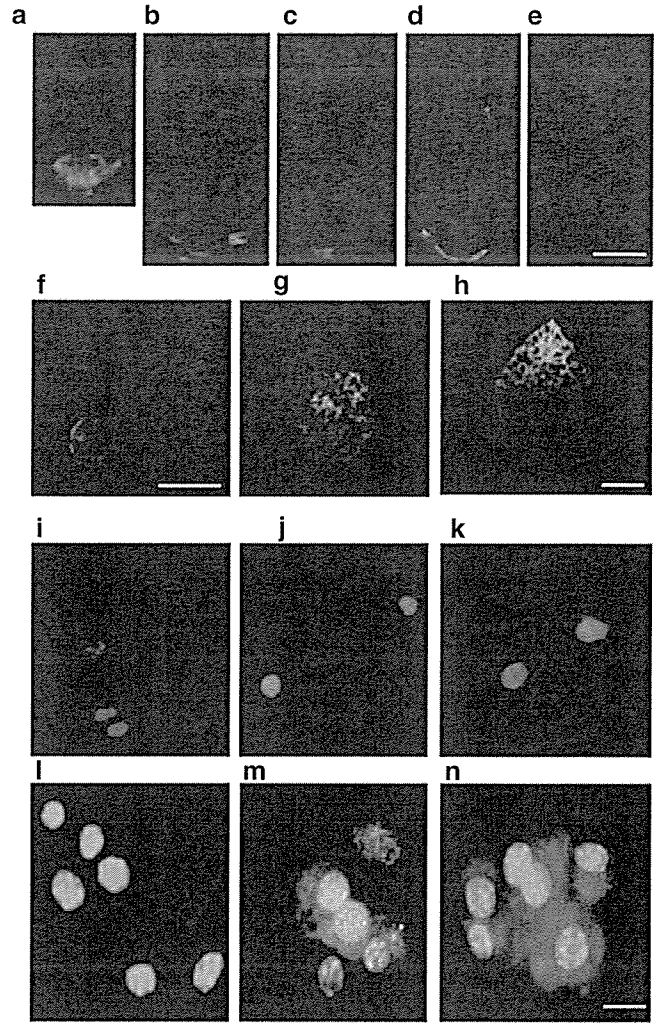


**Figure 2. CD133 expression appears earlier than versican in DP.** (**a–h**) During hair development, (**a**, **b**) hair follicles at stages 2 and 3 express CD133, but (**c**, **d**) versican was not detected until stages 4–5, when both proteins were present in the DP. (**e**) After stage 6, the expression of CD133 was lost but versican was still present. Skin sections of embryos, neonates, and 4-week-old mice were double-stained with anti-CD133 antibody (red) and anti-versican antibody (green). Hair follicles of E16.5 (**a**, stage 3), E17.5 (**b**, stage 4), E18.5 (**c**, stage 5), P0 (**d**, stages 5–6), and P1 (**e**, stage 6) mice. DPs of pelage hairs at early anagen stage (**f**) and vibrissae at early anagen stage (**g**) from 4-week-old mice showed CD133 expression, but the DPs from vibrissae at the late second anagen (**h**) did not. (**a–h**) The bars represent 100 $\mu$m. After isolation by sorting, cultured CD133 (+)/versican (−) cells proliferated and began to express versican. Sorted cells from dorsal skin of E16.5 embryos were either stained (**i–k**) immediately or (**l–n**) after culture for 3 days. Cells were stained with (red in **i**, **l**) anti-CD133 antibody, and (green in **j**, **k**, **m**, **n**) anti-versican antibody. (**i**, **j**) Three-day cultures of CD133 (+)/versican (−) cells began to express (**m**) versican but lost expression of (**l**) CD133. In contrast, (**k**) CD133 (−) versican (+) cells proliferated and still expressed (**n**) versican after 3 days of cultivation. (**i–n**) The bars represent 10 $\mu$m.

**CD133 (+) cells from both embryo- and adult skin-induced hair growth *in vivo***

Hair follicle reconstructive experiments were performed to examine whether CD133 (+) cells of the skin possessed hair follicle-inducing ability. The dorsal skin of C57BL/6 E17.5

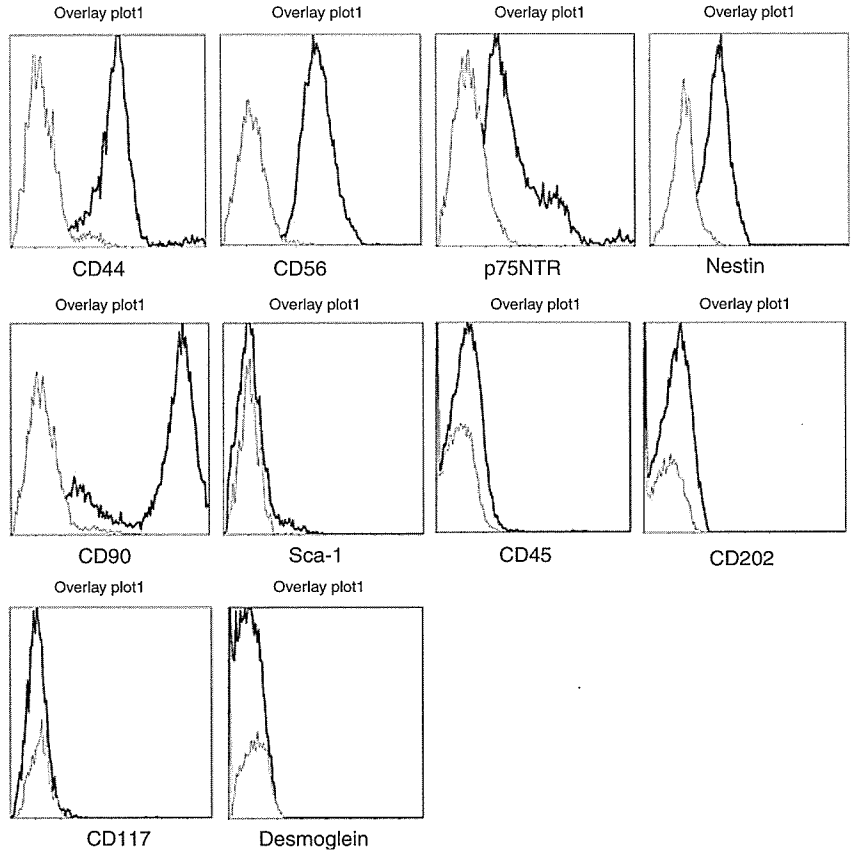


**Figure 3. Flow cytometric analysis of CD133 (+) cells in embryonic skin.** Dermal cells from E16.5 mice were analyzed by flow cytometry. The gated CD133 (+) population is drawn as the bold line in each histogram. Positive staining patterns by anti-CD44, CD56/neural cell adhesion molecule, and p75NTR antibodies showed that the CD133 (+) cells had DP characteristics.

embryos was trypsinized and CD133 (+) cells were isolated by a cell sorter. Epidermal cells were obtained from Balb/c (E17.5) embryos in separate experiments. Mixtures of CD133 (+) and epidermal cells, in a volume of 50 $\mu$l, were injected subcutaneously into athymic nude mice. Two weeks after injection, the combination of CD133 (+) cells ($1 \times 10^5$) and epidermal cells ($5 \times 10^5$) reconstituted new hairs (Figure 5a). In contrast, the combination of CD133 (−) cells and epidermal cells failed to induce hair growth (Figure 5b). Whole dermal cells ($1 \times 10^6$) combined with epidermal cells were injected as a positive control (Figure 5c). No hair grew when CD133 (+) cells only or epidermal cells only were injected (data not shown). When epidermal cells collected from C57BL/6 (E17.5) were used instead of Balb/c embryos, pigmented hairs were formed (Figure 5d, f, g and i). We also injected the cell combinations into muscle in which the blood supply was more abundant than in subcutaneous tissue. The combination of CD133 (+) cells with epidermal cells (Figure 5d) and whole dermal cells ($1 \times 10^6$) with epidermal cells (Figure 5f) induced hair growth. Again, the combination of CD133 (−) cells with epidermal cells failed to induce hair growth (Figure 5e), suggesting that the failure of CD133 (−) cells to induce hair follicles was not due to environmental differences between transplantation sites, but rather to the lack of the hair-inducing ability of the transplanted cells. To examine whether CD133 (+) cells of adult skin could induce hair growth, CD133 (+) cells ($1 \times 10^5$) were obtained from 8-week-old-adult mice depilated 6 days previously. As CD133 (+) cells scarcely exist in adult skin at 0.4% (Table 1), the depilation procedure was required to collect sufficient cells for hair reconstitution. The combination of these CD133 (+) cells and epidermal cells also induced hair growth (Figure 5g), but at relatively low efficiency compared to embryonic derived CD133 (+) cells. CD133 (−) cells from adult skin with epidermal cells failed to induce any hair growth (Figure 5h).

To prove that the grafted CD133 (+) cells repopulated in the DP, CD133 (+) cells were isolated from Rosa26-transgenic (LacZ expressing) or GFP-transgenic (GFP expressing) embryos. After 2 weeks, LacZ or GFP-positive cells were found in the DP of the reconstructed hair follicles, respectively (Figure 5i and j). Interestingly, the grafted CD133 (+) cells appeared mainly in the DP of the newly formed hair follicles, although small populations of LacZ- or GFP-positive cells were observed in the dermal sheath.

**Cultured CD133 (+) cells of adult could induce hair growth**

Recently, multipotent skin-derived precursors (SKPs) have been reported to reside in DP (Toma *et al.*, 2001; Fernandes *et al.*, 2004). We wanted to know whether CD133 (+) cells

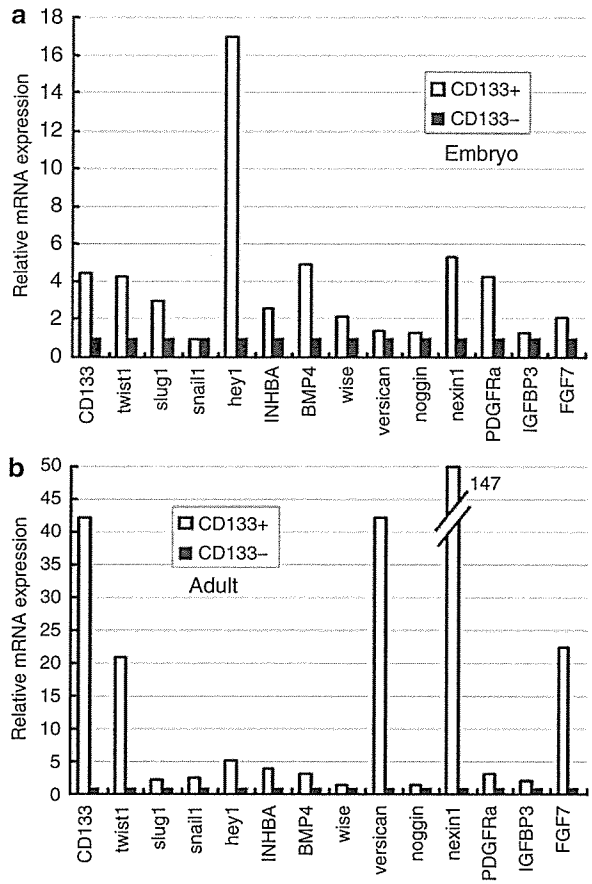


**Figure 4. Gene expression of CD133 (+) cells of embryonic and adult skin corresponds to those of DP cells from the anagen stage.** Quantitative PCR was carried out using samples from CD133 (+) cells of (**a**) E16.5 and (**b**) induced anagen stage from 8-week-old mice. Each cDNA of CD133 (+) and CD133 (−) fractions of the two groups was amplified using several sets of primers as follows: *twist1*, *slug1*, *snail1*, *hey1* (hairy-related transcription factor 1), *INHBA* (inhibin β-A), *BMP4* (bone morphogenic protein 4), *wise* (wnt signaling modulator), *CD133*, *versican*, *noggin*, *nexin1*, *PDGFRα* (platelet-derived growth factor receptor, α), *IGFBP3* (insulin-like growth factor-binding protein 3), *FGF-7* (fibroblast growth factor 7) and *β-actin*. The expression level of the mRNA of each gene was normalized by the *β-actin* gene. The relative expression levels between the CD133 (+) and CD133 (−) samples were shown in the graphs. The CD133 (+) cells both from embryos (**a**) and adult mice (**b**) expressed several genes at least twice as strongly as CD133 (−) cells. The strongly expressed genes in CD133 (+) cells were consistent with those reported as highly transcribed ones in DP cells (Fernandes *et al.*, 2004, Rendl *et al.*, 2005).

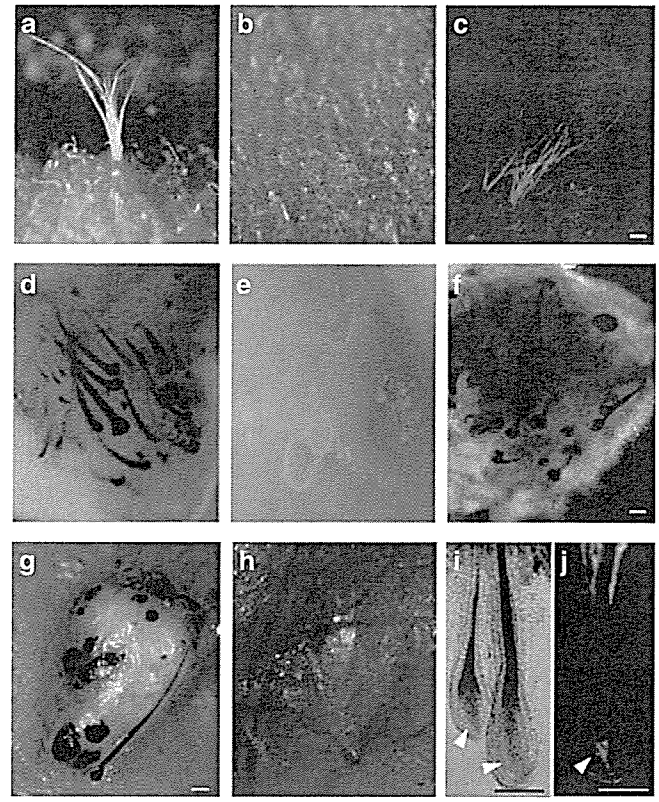


**Figure 5. Skin-derived CD133 (+) cells from embryos and adults induce hair growth *in vivo*.** Dermal cells were collected from (**a–f**) C57BL/6 E17.5 embryos, (**g, h**) 8-week-old mice with 6 days after depilation, (**i**) Rosa-26 E17.5 embryos, (**j**) and GFP-transgenic E17.5 embryos. Epidermal cells were obtained from (**a–c**) Balb/c E17.5 and (**d–j**) C57BL/6 E17.5 mice. Cell mixtures of the dermal fraction and epidermal cells were injected (**a–c**) subcutaneously or (**d–j**) intramuscularly into athymic nude mice. After 14 days (**a**) CD133 (+) cells from embryos induced new hairs, (**c**) similarly to the positive control, but (**b**) CD133 (−) cells did not. (**d–f**) The same results were observed for intramuscular transplantation experiment using pigmented epidermal cells. (**g**) CD133 (+) cells from the DP of an adult mouse also showed hair follicle-inducing ability, but (**h**) CD133 (−) cells did not. (**i, j**) Transplanted CD133 (+) cells from the skin of Rosa26 or GFP-transgenic mouse were found to localize mainly in the DP of newly produced hair (arrowheads) with a few cells localized to the dermal sheath. (**a**) CD133 (+) cells plus epidermal cells, (**b**) CD133 (−) cells plus epidermal cells, (**c**) whole dermal cells plus epidermal cells (positive control), (**d**) CD133 (+) cells plus epidermal cells, (**e**) CD133 (−) cells plus epidermal cells, (**f**) whole dermal cells plus epidermal cells, (**g**) CD133 (+) cells from adult skin plus epidermal cells, (**h**) CD133 (−) cells from adult skin plus epidermal cells, (**i**) CD133 (+) cells from Rosa26 embryos plus epidermal cells (LacZ staining), (**j**) CD133 (+) cells from GFP-transgenic embryos plus epidermal cells. (**h, i**) Cells with blue staining after x-gal staining and green fluorescence were observed in the DP and dermal sheath. All bars represent 100 μm.

showed the same growth characteristics as SKPs. CD133 (+) cells were obtained from the scalp skin of 8-week-old mice, depilated 6 days before. The cells were cultivated in floating culture condition, the same procedure used for obtaining SKPs (DMEM/F12 medium containing 2% B27, epidermal growth factor, basic fibroblast growth factor). Although dissociated CD133 (+) cells from adult mice formed spheres (Figure 6a), the growth rate was much slower than that for SKPs. The first passage occurred after one month, and the second passage was performed yet 1 month later for CD133 (+) spheres. The results of immunostaining with anti-Sca-1 antibody showed a phenotypical difference between the two kinds of spheres; SKPs produced Sca-1 (Figure 6b), whereas spheres of CD133 (+) did not (Figure 6a).

Hair follicle reconstructive experiments showed that 20 spheres from cultured CD133 (+) cells with embryonic epidermal cells ($5 \times 10^5$) gave rise to 5–10 new hairs when they were implanted into nude mice (Figure 6c), whereas 20 spheres of SKPs with embryonic epidermal cells failed to induce any hair growth (Figure 6d). These results indicated

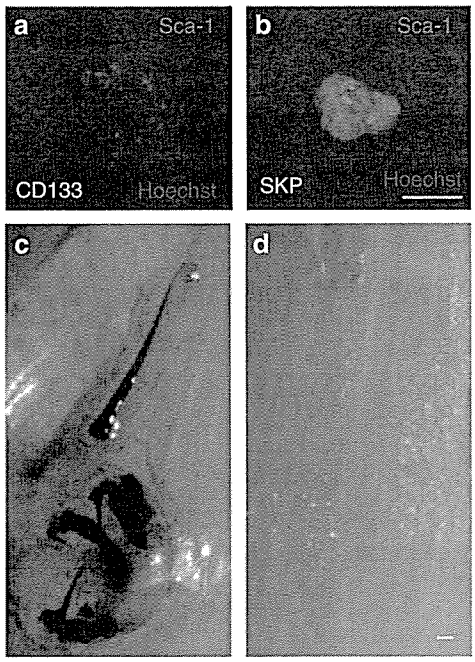


**Figure 6. The spheres from CD133 (+) cells reveal hair-inducing activity.** Freshly isolated CD133 (+) cells from adult skin were cultivated within the defined medium for neuropheres under floating culture conditions. (**a**) The cultivated spheres from the second passage from CD133 (+) cells did not produce Sca-1, but (**b**) the sphere from SKPs did stain positively for Sca-1, as reported previously (Toma *et al.*, 2001). Nuclei were counterstained with Hoechst dye. The hair follicle reconstructive experiments showed that (**c**) the spheres from CD133 (+) cells induced hair growth with epidermal cells, but (**d**) the spheres from SKPs did not. All spheres were cultured and used at second passage. All bars represent 100 $\mu$m.

that CD133 (+) cells retained their hair follicle-inducing ability even after the cultivation.

## DISCUSSION

This study indicates that hair follicle-inducing cells of both embryo and adult produce a membranous protein, CD133. This is the first report that DP cells express CD133 during the early anagen stage and that CD133 (+) cells in the skin possess the ability to induce new hair follicles.

Prior studies for inducing hair follicles have used whole dermal cells of embryonic dorsal skin or isolated DP of vibrissae as the dermal component. It is of note that hair follicle-inducing cells express CD133, because they can thus be selected out from dissociated cells. In *in vivo* hair induction experiments, whole dermal cells from E16.5 to P1 (on the second day of birth) mice (Weinberg *et al.*, 1993; Kishimoto *et al.*, 2000; Zheng *et al.*, 2005) have been used because, after P2 (third day of life) until the end of the first telogen stage of the hair cycle (3 weeks after birth), the dorsal dermal cells lose their hair follicle-inducing ability. This phenomenon probably reflects the number of CD133 (+) cells present during hair morphogenesis in the back skin. In earlier transplantation experiments (Weinberg *et al.*, 1993; Zheng *et al.*, 2005), more than 1 x $10^6$ whole dermal cells were used; however, our experiments required only 1 $\times$ $10^5$ CD133 (+) cells for hair follicle induction (minimum number was 2 $\times$ $10^4$). As the rate of CD133 (+) cells was estimated for 2% (E17.5) of the skin in our data (Table 1), one million dermal cells might contain 2 $\times$ $10^4$ CD133 (+) cells. This number of CD133 (+) cells is equivalent to our minimum requirement for hair follicle induction. Although numerous hair follicles on P0 mice are before stage 4, almost all hair follicles on P2 mice have entered stages 6–8 anagen (Peters *et al.*, 2002), a time that coincides with the downregulation of CD133 expression in DP cells (Figure 1). In fact, flow cytometry analysis showed that the percentage of CD133 (+) cells in the dorsal skin dwindles away after birth (Table 1). Therefore, the presence of CD133 (+) cells in DP may be an indicator of their hair follicle-inducing capability.

In our immunocytostaining results, the dermal condensate/papilla was shown to produce CD133 before versican during the anagen stage. When GFP-positive cells were collected from versican-GFP transgenic mice, it was reported that versican-expressing DP cells have hair-inducing ability (Kishimoto *et al.*, 1999, 2000). In this study, we showed that CD133 (+) cells produce versican after a period of culture, indicating the probability that versican(+) cells with hair follicle-inducing ability are the same population as CD133 (+) cells. CD133 is therefore useful for collecting native, live hair follicle-inducing cells from non-transgenic animals, because it is a cell surface protein.

This marker, CD133, a pentaspan transmembrane glycoprotein, was first described as a marker for human hematopoietic stem cells (Weigmann *et al.*, 1997; Yin *et al.*, 1997). Many other studies provided evidence that this orphan receptor is expressed on various tissue stem/progenitor cells, such as neuronal (Uchida *et al.*, 2000), endothelial (Peichev *et al.*, 2000) lineage, kidney (Bussolati *et al.*, 2005), prostate (Richardson *et al.*, 2004), and cancer cells (Singh *et al.*, 2003). The biological function of CD133 has been explored partially with regard to its participation in lipid rafts on the cell surface (Roper *et al.*, 2000), its contribution to the protrusion of epithelial cells and the release of these protrusions as extracellular membrane particles (Weigmann *et al.*, 1997; Marzesco *et al.*, 2005). Because DP cells produce CD133, we first suspected that the CD133 (+) cells might contain tissue stem cells. However, it is difficult to verify this because, the CD133 (+) cells of DP appear periodically and do not exist in the hair follicles during their resting phase.

The CD133 (+) cells of embryonic skin express CD44, neural cell adhesion molecule/CD56, and p75NTR (Figure 3). As DP cells are already confirmed to be positive for the three proteins (Muller-Rover *et al.*, 1998; Botchkareva *et al.*, 1999; Tuhkanen *et al.*, 1999), CD133 (+) cells are shown to produce the same proteins as DP cells do. A recent report proposed that the DP of P4 mice could be defined as a Lef-1 (+) CD34 (−) CD45 $\beta$(−) CD117 (−) population (Rendl *et al.*, 2005). We confirmed that the phenotype of CD133 (+) cells in adult skin was also Lef-1 (+) CD34(−) CD45(−) CD117(−) (data not shown). The CD133 (+) cells may have the characteristics of neural cells, because they produce CD44, neural cell adhesion molecule/CD56, p75NTR, nestin,

and thy-1. Further analysis is required to fully characterize these CD133 (+) cells.

When we compared the gene expression between CD133 (+) cells and CD133 (−) cells by quantitative PCR, the extent of the difference was more exaggerated in adult cells than in the embryonic cells. Several genes were expressed over twice as strongly (CD133 (+) cells *versus* CD133 (−) cells), and they have been reported as the DP signatures (Rendl *et al.*, 2005). Among them, *CD133*, *twist1*, *versican*, *nexin1*, and *FGF7* were expressed more than 20-fold more strongly in the adult. The adult CD133 (+) cells may provide information about the genes responsible for hair follicle induction.

As shown in Figure 6, cultured CD133 (+) cells of adult skin had hair follicle-inducing power. We decided that floating culture conditions to cultivate sphere-like clusters was a desirable choice for maintaining the hair-inducing ability of the CD133 (+) cells. But under these conditions, the CD133 (+) cells proliferated at an extremely slow pace; it took 1 month for each passage. Other cultivating conditions should be surveyed for obtaining large numbers of hair-inducing cells.

The DP harbors both CD133 (+) cells and SKPs but we consider that two types of cells are different on the basis of their production of cell surface markers and their hair follicle-inducing capability. As shown in Figure 3, flow cytometry analysis revealed that CD133 (+) cells are CD56(+) p75NTR(+)Sca-1(−), whereas SKPs are reported to be CD56(−)p75NTR(−)Sca-1(+). Direct observation of stained cells also showed that SKPs are Sca-1(+), whereas spheres of CD133 are Sca-1(−) (Figure 6a and b). Moreover, the two kinds of spheres displayed a clear functional difference; the spheres of CD133 (+) cells could induce hair follicles; SKPs could not.

In summary, we have identified CD133 as a new cell surface marker for detecting and isolating DP cells with hair follicle-inducing ability. The DP cells express the marker in both embryonic and adult hair follicles. The marker might be used as a powerful tool for elucidating the mechanism of hair follicle development/formation.

## MATERIALS AND METHODS

### Mice and cell preparation

C57BL/6, Balb/c (Clea Japan, Tokyo, Japan), GFP-transgenic mice (gift from Dr M. Okabe, Univ. of Osaka, Japan), and Rosa26-transgenic mice (gift from Drs H Niwa and K Nakao, RIKEN, Kobe, Japan) were maintained in sun protection factor conditions at the animal facilities. Animal studies were conducted according to protocols approved by the International Medical Center of Japan. Embryonic day (E) 13.5–18.5 embryos were obtained by Cesarean section. Skin was harvested from 4 to 8-week-old mice and from neonatal mice on P0, P1, P5, and P11. To obtain dermal cells, embryonic, neonatal back, and adult caudal skin was stripped, minced in DMEM containing 0.25% of trypsin, and incubated for 1 hour at 37°C. Single-cell suspensions were rinsed with phosphate-buffered saline (PBS) and incubated in DMEM containing 5% fetal bovine serum for 1 hour, then used for the hair inductive experiment, reverse transcription PCR and flow cytometry analysis. For preparing cell suspensions of epidermis, embryonic (E17.5) back skin was harvested and treated with 1,000 U/ml dispase (Invitrogen, Carlsbad, CA) for 4 hour at 4°C, and then separated into epidermis and dermis. Peeled epidermis was incubated in 0.25% trypsin-EDTA (Invitrogen) for 30 minutes at 37°C. Cells were washed, suspended in KBM-2 (Cambrex, Walkersville, MD), and then used for the hair follicle inductive experiment.

### Immunohistochemistry

Embryonic, neonatal, adult back skin, and adult vibrissae were sectioned (10 $\mu$m thick) using a cryostat. The sections were incubated with primary antisera to CD133 (eBioscience, San Diego, CA, clone13A4, 1:150) for 1 hour at RT. After washing with PBS, the sections were immersed in PBS containing 2% $H_2O_2$ for 30 minutes at RT. The secondary antibody, HRP-conjugated anti-rat IgG (Amersham Bioscience, Little Chalfont, UK, 1:100) was applied to the sections and incubated for 1 hour at RT with Hoechst dye for nuclear staining. Positive reactions were enhanced using the tyramide signal amplification system (Molecular Probes, Eugene, OR) following the manufacturer's instructions, and visualized with Alexa Fluor 594. For double staining experiments, sections were first incubated with antiserum to CD133 and versican (Chemicon, Temecula, CA, polyclonal no. AB1033). After enhancement with Alexa594-conjugated tyramide (CD133 (+) cells appeared red), Alexa Fluor 488-conjugated anti-rabbit IgG (Molecular Probes) (versican-positive cells appeared green) was applied to the slides for 20 minutes at RT. Alternatively, the sections were incubated with a primary antibody to CD133 (Abcam, UK, polyclonal, 1:20) overnight at 4°C, followed by a secondary antibody, Alexa 594 conjugated anti-rabbit IgG (Molecular Probes, 1:400) for 30 minutes at RT. The slides were mounted with Gel/mount containing an anti-fading reagent (Biomeda, Foster City, CA) and observed under a BX51 fluorescent microscope (Olympus, Tokyo, Japan).

### Cell sorting

Freshly obtained single-cell suspensions were incubated with biotin-conjugated anti-CD133 antibody (eBioscience, clone13A4) for 30 minutes at 4°C followed by the incubation for 15 minutes at 4°C with PE-conjugated streptavidin (BD Bioscience, San Jose, CA). Following staining, the PE-positive cell fraction was sorted using an EPICS ALTRA flow cytometer (Beckman Coulter, Fullerton, CA). Sorted cells were used for hair induction experiments, and cell culturing. For gene expression analysis, CD133 (+) and CD133 (−) cells were separated magnetically. Magnetic labeling of cells was followed after incubation with the primary antibody. Cells were washed and incubated with magnetic beads coated by anti-biotin antibody (Miltenyi Biotec GmBH, Bergisch Gladbach, Germany) for 15 minutes at 4°C. CD133 (+) and CD133 (−) fractions were sorted by an AutoMacs™ (Miltenyi Biotec).

### Cell culture and immunocytochemistry

Sorted cells were seeded into 96-well low-binding plates (Nalgen-unc, Chester, NY) at 2,000 cells/well with Papilla Cell Growth Medium (TOYOBO, Japan) containing 10% fetal bovine serum. Cells were cultured for 3 days, and then stained after a cytospin step for 1 minute at 700 r.p.m. Cells on slides were fixed with 4% paraformaldehyde, 0.2% picric acid in PBS. For intracellular staining, fixed specimens were immersed in cold acetone. Immuno-staining was performed using antibodies against mouse CD133

(raised in rat) and versican (raised in rabbit). Visualization was performed using Alexa fluor 594-conjugated anti-rat antibody (Molecular Probes), and Alexa Fluor 488-conjugated anti-rabbit antibody (Molecular Probes), as described above. Cell sorting was performed as described above.

### Gene expression analysis

One microgram of total RNA was extracted from the sorted CD133 (+) cells of 8 embryos (E16.5) and 10 adult mice (8-week-old) depilated 6 days before the preparation. Negatively sorted cells of each sample were also used as CD133 (−) fraction. Collected cells were treated with Isogen (Wako Chemicals, Japan) and reverse transcribed into cDNA using SuperSCRIPT II (Invitrogen) following the manufacturer's instructions. After reverse transcription, 100 ng of cDNA was used for real-time quantitative PCR, performed with ABI PRISM 7700 Sequence Detector (Perkin Elmer, Wellesley, MA) and the SYBR green (SYBR Premix Ex Taq, Takara, Japan). Primers are listed on Supplementary Data. Amplification included initial denaturation at 95°C for 10 seconds, 50 cycles of denaturation at 95°C for 10 seconds, annealing at 60°C (67°C, only the reaction with primers of CD133) for 30 seconds. Data were normalized to expression of the housekeeping gene $\beta$-actin. Expression level of mRNA of each gene was calculated according to the method reported in the past (Pfaffl, 2001).

### Flow cytometric analysis

Cell suspensions from skin were prepared as described previously. Antibodies used in the present experiment were: anti-neural cell adhesion molecule (MAB310), anti-p75NTR (AB1554) from Chemicon, anti-nestin (Rat401), Thy-1 (53-2.1), CD45 (30-F11), CD117 (2B8), desmoglein (62) from BD Bioscience, and anti-CD133 (13A4), CD44 (IM7), Sca-1 (D7), Tie-2 (TEK4) from eBioscience. When we used anti-nestin antibodies, cells were fixed and permeabilized with IntraPrep (Beckman Coulter). Cells from dorsal skin of E16.5 to E18.5, P1 and P5 mice and from the scalp of 8-week-old mice before and after depilation were prepared for determining the relationship between CD133 (+) cells and hair formation. Analysis was performed with an EPICS XL flow cytometer (Beckman Coulter), and data were analyzed with EXPO32 software (Beckman Coulter).

### Formation of spheres from CD133 (+) cells

To cultivate the CD133 (+) cells under floating conditions, we obtained CD133 (+) cells by sorting and cultured them in a defined medium as described previously (Toma *et al.*, 2001; Kawase *et al.*, 2004). Briefly, skin from 8-week-old mice, depilated 6 days previously, was stripped, minced in DMEM containing collagenase, and incubated for 30 minutes at 37°C. Single-cell suspensions of CD133 (+) cells obtained by sorting were rinsed with PBS and cultured under floating condition in DMEM/F12 (1:1) medium (Invitrogen) containing 2% B-27 supplement (Invitrogen), epidermal growth factor (10 ng ml, R&D systems, Minneapolis, MN), and basic fibroblast growth factor (20 ng ml, R&D systems) using a low-cell-binding plate (Nalgenunc). For passage, spheres were collected by centrifugation, and treated with Accumax (Innovative Cell Technologies, San Diego, CA) for 5 minutes at RT, rinsed with PBS and then resuspended in fresh medium. SKPs were obtained from the ears of 6- to 8-week-old mice using the same procedure as reported previously (Toma *et al.*, 2001; Kawase *et al.*, 2004). The spheres of CD133 (+) cells and SKPs were examined by immunostaining. Each hair follicle inducing experiment was performed in triplicate.

### *In vivo* induction of hair-growth

Athymic nude mice (Balb/cA Jcl-nu), 7 weeks of age, were purchased from Charles River Japan Inc., Japan. Recipient mice were anesthetized with pentobarbital sodium (1.3 mg/kg). Sorted fractions of CD133 (+) cells, CD133 (−) cells, ($1 \times 10^5$ cells each), spheres from CD133 (+) cells (20 spheres each), SKPs (20 spheres each) and whole dermal cells ($1 \times 10^6$ cells) were centrifuged, resuspended in KBM-2 media with epidermal cells ($5 \times 10^5$ cells each) in a volume of 50 $\mu$l, using 25-gauge needle for injection into the intradermal, subcutis or muscle (gluteus maximus muscle) of nude mice. After 2 weeks, the skin or muscle containing trichogenic cells were harvested. The newly formed hair follicles were observed under a SZX12 stereomicroscope and an IX70 light microscope (Olympus).

### X-gal staining

Harvested trichogenic cells were stained with X-gal to detect any dermal contamination from Rosa26 mice. The cells were fixed with 4% paraformaldehyde and 0.5% glutaraldehyde in PBS for 30 minutes and stained for 6 hours at RT with 5 mM $K_3Fe(CN)_6$, 5 mM $K_4Fe(CN)_6$, 2 mM $MgCl_2$, and 1 mg/ml X-gal in PBS (pH 7.2).

### CONFLICT OF INTEREST

The authors state no conflict of interest.

### ACKNOWLEDGMENTS

We thank M Komine for helpful discussion, Y Nagasaka for technical assistance with flow cytometry, T Takeda and S Yoshitake for help in the *in vitro* experiments. This work was supported by Grant-in-Aid for Scientific Research from the Ministry of Education, Science, Sport, Culture and Technology, and from the Ministry of Health, Labour and Welfare of Japan.

### SUPPLEMENTARY MATERIAL

**Table S1.**

### REFERENCES

Botchkarev VA, Kishimoto J (2003) Molecular control of epithelial-mesenchymal interactions during hair follicle cycling. *J Investig Dermatol Symp Proc* 8:46–55

Botchkareva NV, Botchkarev VA, Chen LH, Lindner G, Paus R (1999) A role for p75 neurotrophin receptor in the control of hair follicle morphogenesis. *Dev Biol* 216:135–53

Bussolati B, Bruno S, Grange C, Buttiglieri S, Deregibus MC, Cantino D *et al.* (2005) Isolation of renal progenitor cells from adult human kidney. *Am J Pathol* 166:545–55

du Cros DL, LeBaron RG, Couchman JR (1995) Association of versican with dermal matrices and its potential role in hair follicle development and cycling. *J Invest Dermatol* 105:426–31

Fargeas CA, Joester A, Missol-Kolka E, Hellwig A, Huttner WB, Corbeil D (2004) Identification of novel Prominin-1/CD133 splice variants with alternative C-termini and their expression in epididymis and testis. *J Cell Sci* 117:4301–11

Fernandes KJ, McKenzie IA, Mill P, Smith KM, Akhavan M, Barnabe-Heider F *et al.* (2004) A dermal niche for multipotent adult skin-derived precursor cells. *Nat Cell Biol* 6:1082–93

Kawase Y, Yanagi Y, Takato T, Fujimoto M, Okochi H (2004) Characterization of multipotent adult stem cells from the skin: transforming growth factor-beta (TGF-beta) facilitates cell growth. *Exp Cell Res* 295:194–203

Kishimoto J, Burgeson RE, Morgan BA (2000) Wnt signaling maintains the hair-inducing activity of the dermal papilla. *Genes Dev* 14:1181–5

Kishimoto J, Ehama R, Wu L, Jiang S, Jiang N, Burgeson RE (1999) Selective activation of the versican promoter by epithelial–mesenchymal interactions during hair follicle development. *Proc Natl Acad Sci USA* 96:7336–41

Marzesco AM, Janich P, Wilsch-Brauninger M, Dubreuil V, Langenfeld K, Corbeil D *et al.* (2005) Release of extracellular membrane particles carrying the stem cell marker prominin-1 (CD133) from neural progenitors and other epithelial cells. *J Cell Sci* 118:2849–58

Muller-Rover S, Handjiski B, van der Veen C, Eichmuller S, Foitzik K, McKay IA *et al.* (2001) A comprehensive guide for the accurate classification of murine hair follicles in distinct hair cycle stages. *J Invest Dermatol* 117:3–15

Muller-Rover S, Peters EJ, Botchkarev VA, Panteleyev A, Paus R (1998) Distinct patterns of NCAM expression are associated with defined stages of murine hair follicle morphogenesis and regression. *J Histochem Cytochem* 46:1401–10

Paus R, Foitzik K (2004) In search of the "hair cycle clock": a guided tour. *Differentiation* 72:489–511

Paus R, Muller-Rover S, Van Der Veen C, Maurer M, Eichmuller S, Ling G *et al.* (1999) A comprehensive guide for the recognition and classification of distinct stages of hair follicle morphogenesis. *J Invest Dermatol* 113:523–32

Peichev M, Naiyer AJ, Pereira D, Zhu Z, Lane WJ, Williams M *et al.* (2000) Expression of VEGFR-2 and AC133 by circulating human CD34(+) cells identifies a population of functional endothelial precursors. *Blood* 95:952–8

Peters EM, Botchkarev VA, Muller-Rover S, Moll I, Rice FL, Paus R (2002) Developmental timing of hair follicle and dorsal skin innervation in mice. *J Comp Neurol* 448:28–52

Pfaffl MW (2001) A new mathematical model for relative quantification in real-time RT-PCR. *Nucleic Acids Res* 29:e45

Rendl M, Lewis L, Fuchs E (2005) Molecular dissection of mesenchymal–epithelial interactions in the hair follicle. *PLoS Biol* 3:e331

Reynolds AJ, Jahoda CA (1992) Cultured dermal papilla cells induce follicle formation and hair growth by transdifferentiation of an adult epidermis. *Development* 115:587–93

Richardson GD, Robson CN, Lang SH, Neal DE, Maitland NJ, Collins AT (2004) CD133, a novel marker for human prostatic epithelial stem cells. *J Cell Sci* 117:3539–45

Roper K, Corbeil D, Huttner WB (2000) Retention of prominin in microvilli reveals distinct cholesterol-based lipid micro-domains in the apical plasma membrane. *Nat Cell Biol* 2:582–92

Schmidt-Ullrich R, Paus R (2005) Molecular principles of hair follicle induction and morphogenesis. *Bioessays* 27:247–61

Singh SK, Clarke ID, Terasaki M, Bonn VE, Hawkins C, Squire J *et al.* (2003) Identification of a cancer stem cell in human brain tumors. *Cancer Res* 63:5821–8

Toma JG, Akhavan M, Fernandes KJ, Barnabe-Heider F, Sadikot A, Kaplan DR *et al.* (2001) Isolation of multipotent adult stem cells from the dermis of mammalian skin. *Nat Cell Biol* 3:778–84

Tuhkanen AL, Agren UM, Tammi MI, Tammi RH (1999) CD44 expression marks the onset of keratinocyte stratification and mesenchymal maturation into fibrous dermis in fetal human skin. *J Histochem Cytochem* 47:1617–24

Uchida N, Buck DW, He D, Reitsma MJ, Masek M, Phan TV *et al.* (2000) Direct isolation of human central nervous system stem cells. *Proc Natl Acad Sci USA* 97:14720–5

Weigmann A, Corbeil D, Hellwig A, Huttner WB (1997) Prominin, a novel microvilli-specific polytopic membrane protein of the apical surface of epithelial cells, is targeted to plasmalemmal protrusions of non-epithelial cells. *Proc Natl Acad Sci USA* 94:12425–30

Weinberg WC, Goodman LV, George C, Morgan DL, Ledbetter S, Yuspa SH *et al.* (1993) Reconstitution of hair follicle development *in vivo*: determination of follicle formation, hair growth, and hair quality by dermal cells. *J Invest Dermatol* 100:229–36

Yin AH, Miraglia S, Zanjani ED, Almeida-Porada G, Ogawa M, Leary AG *et al.* (1997) AC133, a novel marker for human hematopoietic stem and progenitor cells. *Blood* 90:5002–12

Zheng Y, Du X, Wang W, Boucher M, Parimoo S, Stenn K (2005) Organogenesis from dissociated cells: generation of mature cycling hair follicles from skin-derived cells. *J Invest Dermatol* 124:867–76

*Journal of Drug Targeting*, July 2006; 14(6): 413–424

informa
healthcare

# Photochemical enhancement of transgene expression by polymeric micelles incorporating plasmid DNA and dendrimer-based photosensitizer

NOBUHIRO NISHIYAMA[1], ARNIDA[2], WOO-DONG JANG[2], KOTOE DATE[2], KANJIRO MIYATA[2], & KAZUNORI KATAOKA[1,2,3,4]

[1]*Center for Disease Biology and Integrative Medicine, Graduate School of Medicine, The University of Tokyo, 7-3-1 Hongo, Bunkyo-ku, Tokyo 113-0033, Japan,* [2]*Department of Materials Engineering, Graduate School of Engineering, The University of Tokyo, 7-3-1 Hongo, Bunkyo-ku, Tokyo 113-8656, Japan,* [3]*Core Research Program for Evolutional Science and Technology (CREST), Japan Science and Technology Agency (JST), Tokyo, Japan, and* [4]*Center for NanoBio Integration, The University of Tokyo, 7-3-1 Hongo, Bunkyo-ku, Tokyo 113-8656, Japan*

*(Received 15 November 2005; revised 19 January 2006; in final form 2 February 2006)*

**Abstract**

The development of synthetic gene carriers has recently received much attention; however, they might lack the ability to control the transgene expression. The use of external stimuli for enhancement of the transgene expression may be a promising approach for the site-directed transfection *in vivo*. In this regard, a new technology of "photochemical internalization (PCI)" has recently been reported, in which the endosomal escape of gene carriers is assisted by photodamage of the endosomal membrane with co-incubating photosensitizers. To apply this technology for systemic gene delivery, the development of appropriate carrier systems for both the plasmid DNA (pDNA) and photosensitizer is of crucial importance. Also, the photocytotoxicity accompanied by the photochemical enhancement of the gene expression may need to be reduced. In this study, the combinational formulation of polymeric micelles incorporating pDNA and a dendrimer-based photosensitizer (DP) (dendrimer phthalocyanine (DPc)) was applied in the PCI-mediated transfection *in vitro* and then, estimating its potential utility for *in vivo* applications. The PCI using the polymeric micelle system achieved a remarkable photochemical enhancement of the transgene expression while maintaining an approximate 80% cell viability over a wide range of the DPc concentrations and light doses. Thus, this system may be promising for *in vivo* PCI-mediated gene delivery.

**Keywords:** *Gene therapy, non-viral gene carriers, polymeric micelles, photochemical internalization (PCI), dendrimer*

## Introduction

Recently, non-viral gene carriers based on cationic lipids and synthetic polymers have received much attention as an attractive alternative to viral vectors in gene therapy (Merdan et al. 2002; Ogris and Wagner 2002; Pack et al. 2005). In addition to several advantages, such as safety, simplicity of use and ease of mass production, the variety of chemical designs of the constituent lipids and polymers is a strong motivation to develop novel gene carriers. In particular, considerable efforts have been devoted to the development of biocompatible gene carriers, which might show longevity during blood circulation and effectively accumulate at the target site (Ogris and Wagner 2002; Pack et al. 2005). In this regard, a promising approach is the use of poly(ethylene glycol) (PEG)–polycation block copolymers, since they spontaneously associate with plasmid DNA (pDNA) to form the nano-scaled polyplex micelles, in which the pDNA/polycation polyplex core is surrounded by a dense and hydrophilic PEG palisade (Katayose and Kataoka 1997; Harada-Shiba et al. 2002; Itaka et al. 2003; Miyata et al. 2004; Wakebayashi et al. 2004; Fukushima et al. 2005). Indeed, the polyplex micelles formed between pDNA and PEG–poly(L-lysine)

Correspondence: K. Kataoka, Department of Materials Engineering, Graduate School of Engineering, The University of Tokyo, 7-3-1 Hongo, Bunkyo-ku, Tokyo 113-8656, Japan. E-mail: kataoka@bmw.t.u-tokyo.ac.jp

ISSN 1061-186X print/ISSN 1029-2330 online 
DOI: 10.1080/10611860600834508

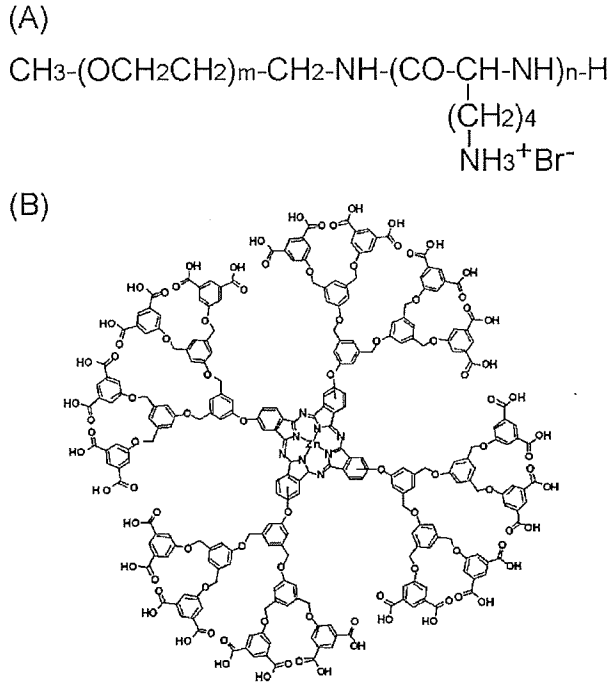


Figure 1. Chemical structures of PEG–PLL block copolymer (A) and DPc (B).

(PEG–PLL) block copolymers (Figure 1(A)) showed an improved stability in proteinous media (Itaka et al. 2003) and prolonged blood circulation in mice (Harada-Shiba et al. 2002). However, the limited transfection ability of the pDNA/PEG–PLL polyplex micelle is a major issue in their applications for *in vivo* gene therapy (Harada-Shiba et al. 2002; Itaka et al. 2003; Miyata et al. 2004). It has been suggested that such a low gene transferring ability of the polyplex micelles might be due to their inefficient transport from the endosome/lysosome to the cytoplasm (Itaka et al. 2003; Miyata et al. 2004).

Other than a high transfection efficiency, site-specific gene transfer has been strongly desired for gene vectors to ensure the safety and effectiveness for *in vivo* gene therapy. However, the existing vectors including viral and non-viral ones still have the problem of non-specific gene transfection. Recently, a smart approach called "photochemical internalization (PCI)" was introduced by Høgset and Berg et al. to overcome both the limited transfection efficiency and the lack of specificity of non-viral gene vectors. The PCI using hydrophilic photosensitizers allows the photochemical disruption of the endosomal/lysosomal membranes, facilitating the cytoplasmic delivery of macromolecular compounds such as genes and proteins (Berg et al. 1999; Høgset et al. 2000, 2002, 2004; Prasmickaite et al. 2001). This approach indeed achieved an appreciable increase in the transfection efficiency upon light illumination under *in vitro* conditions; however, it was accompanied by the problem of photocytotoxicity (Høgset et al. 2000). It should be noted that the photocytotoxicity might not be directly correlated with the photodamage to the endosomal/lysosomal membranes, but the photodamaging of other susceptible organelles may account for the cytotoxicity involved in the PCI (Macdonald and Dougherty 2001; Moan et al. 1994). Hence, the spatially localized photodamage limited to the endosome/lysosome is assumed to lead to the enhanced photochemical transfection with reduced cytotoxicity (Nishiyama et al. 2005). Also, in addition to controlled localization in the intracellular compartment, photosensitizers might need to be systemically delivered to the target tissue to achieve a successful PCI-mediated gene delivery *in vivo*.

In this study, the PCI using polymeric micelles incorporating DPs (dendrimer phthalocyanine (DPc) illustrated in Figure 1(B)) was carried out to enhance the gene transferring ability of the aforementioned pDNA/PEG–PLL polyplex micelle in a light-selective manner (Figure 2). DPc possesses a center phthalocyanine molecule surrounded by a second generation of aryl ether dendrons and 32 carboxyl groups on the periphery of the DPc allow the formation of polyion complex (PIC) micelles through an electrostatic interaction with the PEG–PLL block copolymers

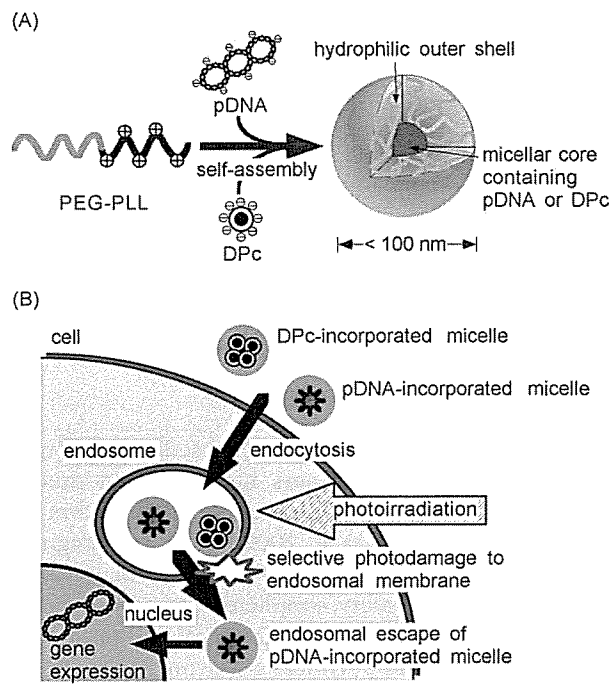


Figure 2. (A) Formation of polymeric micelles through the electrostatic interaction between PEG–PLL and pDNA or DPc. (B) Scheme for itinerary of the pDNA- and DPc-incorporated micelles in the PCI-mediated transfection. Both polymeric micelles are assumed to be taken up by the cell through the endocytic pathway and the localization of the DPc-incorporated micelles in the endosome may allow the selective photodamaging of the endosomal membrane upon photoirradiation, thereby inducing the cytoplasmic delivery of the pDNA-incorporated micelles.

(Stapert et al. 2000; Ideta et al. 2005; Jang et al. 2005). In this strategy, both the pDNA- and DPc-incorporated polymeric micelles are expected to exhibit prolonged blood circulation after intravenous administration and selectively accumulate in the target tissues such as solid tumors as previously reported (Kwon et al. 1994; Nishiyama et al. 2003a,b; Bae et al. 2005). Also, both micelles are assumed to show the same subcellular localization at the target site due to similar particle sizes and surface properties. The control of the localization of the photosensitizers and gene carriers at both the tissue and subcellular levels appears to be a prerequisite for the PCI-mediated gene delivery *in vivo*. Furthermore, the DPc-incorporated micelles may cause highly selective photodamage to the endosomal/lysosomal membranes, because polymeric micelles are assumed to be taken up by the cell through the endocytic pathway (Figure 2(B)). Thus, the combinational use of the pDNA- and DPc-incorporated micelles may be a promising approach to the PCI-mediated gene delivery. In the present study, the feasibility of our strategy was confirmed by the enhanced *in vitro* transfection with limited cytotoxicity under different conditions, thus featuring the possibilities for future *in vivo* applications.

## Materials and methods

### *Materials*

$N^{\varepsilon}$-Z-L-Lysine and bis(trichloromethyl) carbonate (triphosgene), for the synthesis of PEG–PLL, were purchased from Sigma-Aldrich Co., Inc. (St Louis, MO) and Tokyo Kasei Co., Ltd (Tokyo, Japan), respectively. α-Methoxy-ω-amino-poly(ethylene glycol) (MeO–PEG–$NH_2$, MW = 12 kg/mol) was purchased from Nippon Oil and Fats, Co., Ltd. Chemicals for the dendrimer synthesis were purchased from Tokyo Kasei and Sigma-Aldrich. *n*-Pentanol and 1,8-diazabicyclo-(5,4,0)-undec-7-ene (DBU) were purchased from Tokyo Kasei and used without further purification. All solvents for the polymer syntheses were distilled just before use.

A pDNA, pCAcc + Luc, containing a firefly luciferase cDNA driven by a CAG promoter (Niwa et al. 1991) was provided by the RIKEN Bioresource Center (Tsukuba, Japan). pDNA was amplified in competent DH5α *Escherichia coli* and purified by a HiSpeed Plasmid Maxi Kit from Qiagen Co., Inc. (Valencia, CA). Sulfonated aluminum phthalocyanine ($AlPcS_{2a}$) (aluminum phthalocyanine with two sulfonate groups on adjacent phthalate rings) was purchased from Frontier Scientific Co., Inc. (Logan, UT).

### *Polymer synthesis and characterization*

The synthesis of the ionic DPc was performed according to the method reported by Ng's group (Ng et al. 1999). The second generation of dendritic phenol was reacted with 4-nitrophthalonitrile by an alkali-mediated coupling reaction to obtain the corresponding dendritic phthalonitrile, which was then treated with $Zn(OAc)_2$ and DBU in *n*-pentanol to give DPc. The obtained DPc was treated with a THF/$H_2O$ mixture solution containing NaOH to obtain the ionic DPc (MW: 4904). The absorption spectra in an aqueous solution revealed that DPc exhibits a B band absorption at 350 nm and a strong Q band absorption at 685 nm, indicating a monomeric dispersion without agglomerization.

PEG–PLL block copolymers (PEG: MW = 12 kg/mol) having different polymerization degrees of the PLL segment (49 and 73; the code names are 12–49 and 12–73, respectively) were synthesized as previously reported (Harada and Kataoka 1995). Briefly, the *N*-carboxy anhydride of $N^{\varepsilon}$-Z-L-lysine was polymerized from the ω-$NH_2$ group of $CH_3O$–PEG–$NH_2$ in DMF under Ar to obtain PEG–PLL(Z), followed by deprotection of the Z group. The polymerization degree of the PLL segments and the narrowly distributed nature of the synthesized PEG–PLL(Z) were determined by the $^1$H-NMR and the gel permeation chromatography (GPC), respectively.

### *Preparation of DPc-incorporated micelles*

The DPc-incorporated micelles were prepared by mixing DPc and PEG–PLL 12–49 at a stoichiometric charge ratio. In a typical procedure, PEG–PLL was dissolved in a 10 mM $NaH_2PO_4$ solution (0.457 ml) and added to DPc in a 10 mM $Na_2HPO_4$ solution (1.0 ml) to give the solution containing the DPc-incorporated micelles in a 10 mM phosphate buffered solution (pH 7.4). The size and size distribution (polydispersity index) of the micelles were measured by dynamic light scattering (DLS) measurements using a DLS-7000 instrument with a vertically polarized incident beam of 488 nm wavelength from an Ar ion laser (Otsuka Electronics Co., Ltd, Osaka, Japan).

### *Preparation of pDNA/PEG–PLL polyplex micelles*

pDNA and PEG–PLL 12–73 were separately dissolved in a 10 mM Tris–HCl buffer (pH 7.4). The PEG–PLL solution with varying concentrations was then added to the pDNA solution to form the polyplex micelles with different N/P ratios, which denote the ratio of the molar concentration of the cationic amino groups in PEG–PLL to that of the phosphate groups in DNA. The polyplex micelle solution was maintained overnight at ambient temperature before use.

The size and size distribution of the polyplex micelles were measured by the DLS measurement using the DLS-7000. The effect of the N/P ratios on the pDNA condensation in the polyplex micelles was estimated from a decrease in the fluorescence intensity

of ethidium bromide (EtBr) due to the exclusion from the DNA double strand. The polyplex micelle solutions at various N/P ratios were adjusted to 20 μg pDNA/ml with 0.4 μg EtBr/ml by adding 10 mM Tris–HCl buffer containing EtBr. The ratio of the residual molar concentration of EtBr to that of the base pair in pDNA was 0.033. The fluorescence measurements (Ex: 510 nm; Em: 590 nm) were carried out at 25°C using a FP-777 spectrofluorometer from Jasco Co., Ltd (Tokyo, Japan). The results were expressed as the relative fluorescence intensity to the intensity of the free pDNA solution with EtBr.

### In vitro *transfection and cytotoxicity assays*

Human cervical carcinoma HeLa cells or human hepatoma HuH-7 cells (10,000 cells) were seeded and cultured on a 24-well culture plate (BD Bioscience, Franklin Lakes, NJ) for 24 h prior to the transfection (cell seeding density: 1400 cells/cm$^2$). The pDNA/-PEG–PLL polyplex micelle solution prepared at a defined N/P ratio containing 1 μg pDNA and the photosensitizer solutions (i.e. AlPcS$_{2a}$, DPc and DPc-incorporated micelle) with various concentrations were added to the cells in 0.5 ml of Dulbecco's modified Eagle's medium (DMEM) containing 10% fetal bovine serum (FBS), followed by a 6 or 24 h incubation and medium replacement with a fresh one. The culture plates were photoirradiated using a 300 W halogen lamp (fluence rate: 3.0 mW/cm$^2$) equipped with a band-pass filter (400–700 nm) with increased fluence (2.7–8.1 J/cm$^2$). After a 48 h post-incubation, the transfection efficiency and cell viability were examined. In the transfection assay, the cells were lysed and the luciferase activity of the lysate was measured using the Luciferase Assay System (Promega, Madison, WI) and a Lumat LB9507 luminometer (Berthold Technologies, Bad Wildbad, Germany). The results are expressed as light units per milligram of cell protein determined by a BCA assay kit (Pierce, Rockford, IL). On the other hand, the cell viability was evaluated by the 3-(4,5-dimethylthiazol-2-yl)-2,5-diphenyltetrazolium bromide (MTT) (Dojindo Laboratories, Kumamoto, Japan) assay.

## Results and discussion

In this study, we investigated the feasibility of using polymeric micelles as a nanocarrier for the pDNA and photosensitizer in the PCI-mediated gene delivery *in vitro*. As previously described, a simple mixing of pDNA and PEG–PLL results in the formation of the polyplex micelles (Katayose and Kataoka 1997; Itaka et al. 2003). The size and polydispersity indices of the mixtures prepared at various N/P ratios are shown in Figure 3(A) and (B), indicating the formation of the polyplex micelles with sizes of 90–140 nm and a moderate polydispersity over a broad range of N/P ratios (0.5–6). The histogram analysis in the DLS measurement revealed that the polyplex micelles possess a unimodal size distribution (data not shown). Figure 3(C) shows the effect of the N/P ratios

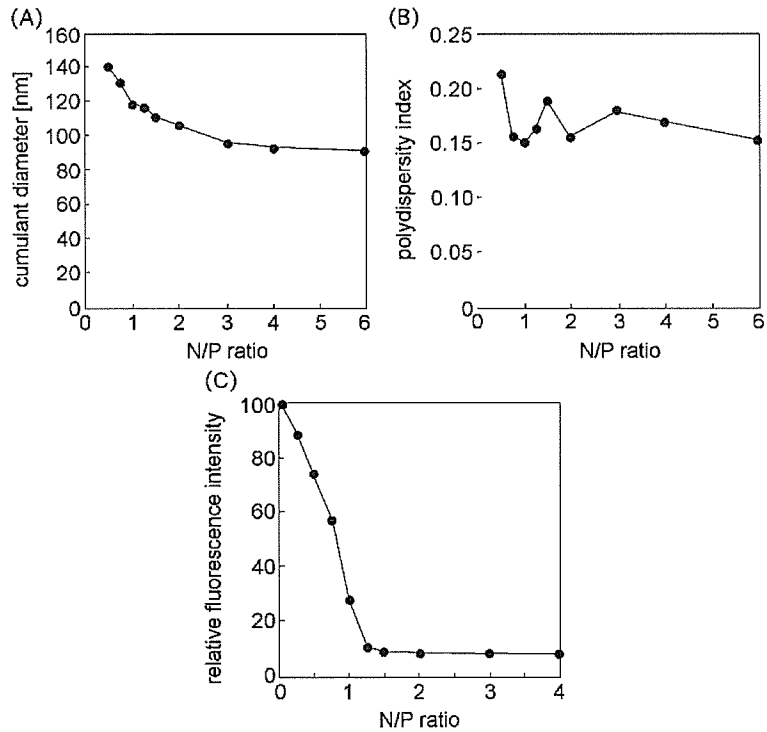


Figure 3. Changes in the cumulant diameter (A), the polydispersity index ($\mu_2/\Gamma^2$) (B) and the fluorescence intensity of EtBr (C) for the pDNA/PEG–PLL polyplex micelles prepared at different N/P ratios.

on the exclusion of EtBr from the pDNA/PEG–PLL complexes. Apparently, the fluorescence intensity of EtBr leveled off above the N/P ratio of 1.2, suggesting this to be a minimum N/P ratio to fully condense pDNA. On the other hand, it is generally difficult to incorporate conventional photosensitizers into nanocarriers, because they have a hydrophobic structure with a large $\pi$-conjugation domain that easily forms aggregates. Recently, we reported DPs as a promising photosensitizer applicable for drug delivery (Nishiyama et al. 2003a,b). DPs have a focal sensitizer core segregated by a 3D dendritic architecture, which might allow effective photochemical reactions even at a high concentration and the periphery with tailored functional groups. Ionic DPs with cationic or anionic peripheral groups show a good solubility in aqueous media and form a PIC micelle with oppositely charged block copolymers (Stapert et al. 2000). We have demonstrated that polymeric micelles incorporating DPs are promising photosensitizer formulations for photodynamic therapy (Ideta et al. 2005; Jang et al. 2005). In the present study, the DPc-incorporated micelles were spontaneously formed through an electrostatic interaction between DPc and PEG–PLL. The DLS measurement revealed that the DPc-incorporated micelles had a diameter of 50 nm with a narrow size distribution (unimodal, polydispersity index ($\mu_2/\Gamma^2$): 0.12). The DPc-incorporated micelles have strong Q-band absorptions at 630 and 685 nm for excitation of the DPc, thus, expecting a deeper tissue penetration of light for *in vivo* applications.

This study's objective is to investigate the feasibility of the PCI-mediated gene delivery using polymeric micelles as nanocarriers for pDNA and DPc. First, the optimal N/P ratio of the pDNA/PEG–PLL polyplex micelles on the photochemical transfection was determined. Figure 4(A) and (B) show the photochemical enhancement of the transfection of the pDNA/PEG–PLL polyplex micelles prepared at the N/P ratio of 1.2 or 2.0 and the concomitant photocytotoxicity, respectively. In this experiment, HeLa cells were photoirradiated at the fluence of 5.4 J/cm$^2$ after a 6 h incubation with the combination of the pDNA- and DPc-incorporated micelles and medium replacement with a fresh one, followed by a 48 h post-incubation. The polyplex micelles prepared at N/P = 1.2 achieved more than a 100-fold photochemical enhancement of the gene expression with 20–25% decreases in cell viability, whereas those prepared at N/P = 2.0 showed only a 10–30-fold gene expression enhancement with comparable decreases in cell viability. Thus, the polyplex micelles prepared at N/P = 1.2 might be more efficient in the PCI-mediated transfection compared with those prepared at N/P = 2.0. It should be noted that naked plasmid did not show any detectable gene transfection, regardless of the utilization of the PCI (data not shown), suggesting the necessity of appropriate gene

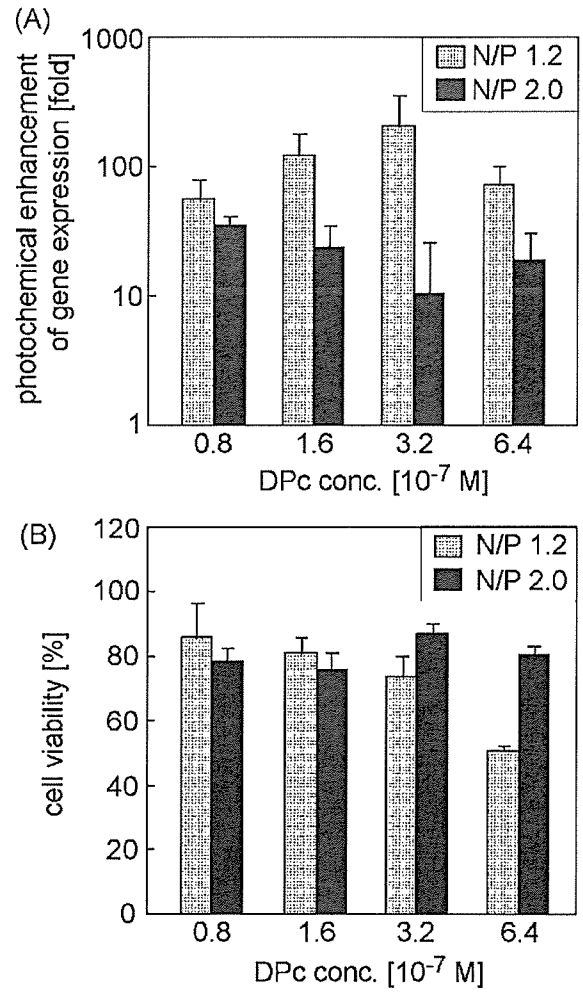


Figure 4. The effect of the N/P ratio of the polyplex micelles on the photochemical enhancement of the gene expression (A) and photocytotoxicity (B) in the PCI-mediated transfection using DPc-incorporated micelle. The light irradiation (fluence: 5.4 J/cm$^2$) was performed 6 h after incubation with the pDNA- and DPc-incorporated micelles, followed by 48 h post-incubation in a fresh medium.

carriers for the PCI-mediated gene delivery. Interestingly, the polyplex micelles prepared at the N/P ratios of 1.2 and 2.0 showed similar transfection efficiencies in the absence of a photosensitizer and light (5,08,000 ± 1,49,000 vs. 4,17,000 ± 1,69,000 RLU/mg protein (mean ± SD)). These results suggest that an excess of PEG PLL might decrease the efficacy of the photochemical transfection. In the PCI-mediated transfection, the efficient cytoplasmic delivery of the polyplex micelles can be achieved by photochemical rupture of the endosomal membrane; therefore, the release of pDNA from the polyplex micelles in the cytoplasm or nuclei may be a rate-limiting process in the gene transfection. The polyplex micelles at N/P = 1.2 are expected to show more efficient pDNA release than those at N/P = 2.0, thereby showing a higher photochemical enhancement of the transfection. Based on these results,

polyplex micelles prepared at N/P = 1.2 were used for further investigations.

The transfection efficiency and cytotoxicity of the polyplex micelles co-incubated with the DPc-incorporated micelles in the presence or absence of light irradiation (fluence: 5.4 J/cm$^2$) are shown in Figure 5(A) and (B), respectively. The same experimental procedures as in Figure 4 were applied in this study. Based on these results, the PCI using the DPc-incorporated micelles achieved a 56–212-fold photochemical enhancement of the transfection of the polyplex micelles while maintaining an approximately 80% cell viability over a wide range of DPc concentrations ($0.4 \times 10^{-7}$–$3.2 \times 10^{-7}$ M) and showed an approximately 50% decrease in viability above the critical DPc concentration ($6.4 \times 10^{-7}$ M). Note that a similar photochemical enhancement of the transfection was observed when 293 T cells were used (data not shown). The maximal transfection level achieved by the PCI using the DPc-incorporated micelles was comparable to that obtained using hydroxychloroquine (hc), which has been demonstrated to be a potent endosomotropic agent (Itaka et al. 2004) (Figure 5(A)). Interestingly, the transfection efficiency of the polyplex micelles decreased as the concentration of the DPc-incorporated micelles increased, particularly under non-irradiated conditions (Figures 5(A) and 6(A)), thus leading to a remarkably high light-selectivity of the gene transfection. Such a DPc concentration-dependent decrease in the transfection efficiency of the polyplex micelles was not observed in the PCI using DPc alone (Figure 7(A)). There may be two possible explanations for this observation. First, the polyplex micelles may compete with the DPc-incorporated micelles in the cellular uptake due to similar particle sizes and surface properties. In Figure 5(A), the molar concentration of the DPc-incorporated micelles was estimated to be comparable to or 20-fold higher than that of the polyplex micelles at the DPc concentration of $2.0 \times 10^{-8}$ or $6.4 \times 10^{-7}$ M, respectively. An increase in the DPc concentration decreases the molar ratio of the pDNA-incorporated micelles to the DPc-incorporated micelles in the medium, leading to a decreased cellular uptake of the pDNA-incorporated micelles. Alternatively, the pDNA- and DPc-incorporated micelles may interact each other, thereby decreasing the transfection efficiency. Indeed, we observed in Figure 4(A) that an excess of PEG–PLL could decrease the transfection efficiency of the polyplex micelles in the PCI-mediated transfcetion. These possibilities may also account for the DPc concentration-dependent decrease in the transfection efficiency.

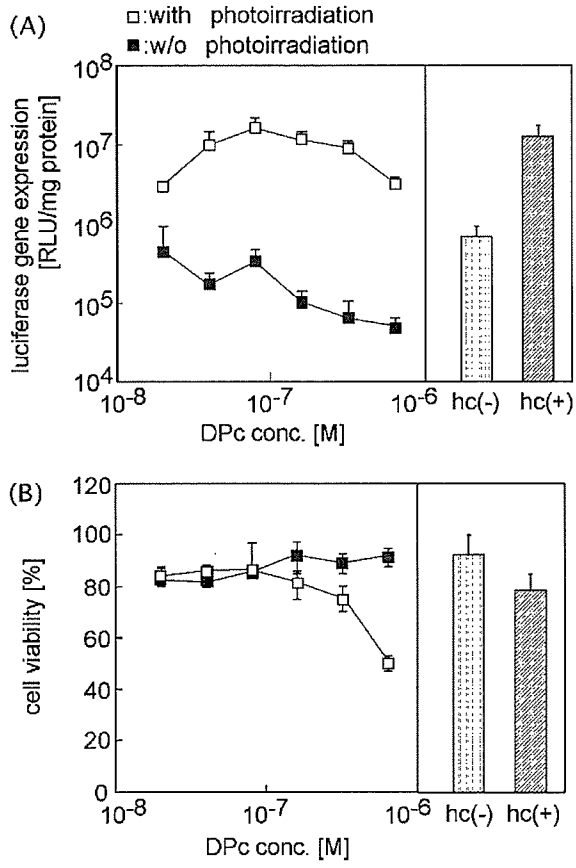


Figure 5. The effect of the DPc concentration on the transfection efficiency (A) and photocytotoxicity (B) in the PCI-mediated transfection using the DPc-incorporated micelles. The light irradiation (fluence: 5.4 J/cm$^2$) was performed 6 h after incubation with the pDNA- and DPc-incorporated micelles, followed by 48 h post-incubation in a fresh medium.

Regarding changes in cell viability in Figure 5(B), a DPc concentration-dependent decrease in cell viability was observed at the DPc concentrations above $1.6 \times 10^{-7}$ M, while a DPc concentration-independent 10–20% decrease in cell viability was observed below $1.6 \times 10^{-7}$ M DPc, regardless of photoirradiation. It is assumed that the DPc concentration-dependent decrease in cell viability observed at the region of high-DPc concentration might be attributable to the photochemical reactions in the PCI-mediated transfection. On the other hand, the 10–20% decrease in cell viability at the lower DPc concentration even without photoirradiation may be inducible by the DPc-incorporated micelles, since the pDNA-incorporated micelles alone did not show an appreciable cytotoxicity (Figures 6(C) and 7(C)). Nevertheless, such a 10–20% decrease in cell viability, of which the mechanisms remain to be clarified yet, is still in a tolerable range and is unlikely to be the serious limitations of this strategy.

The effects of the DPc concentration and fluence on the transfection efficiency of the polyplex micelles, photochemical enhancement of the transfection and photocytotoxicity in the PCI using the DPc-incorporated micelles were completely examined and the results are shown in Figure 6(A)–(C), respectively. Similarly, the PCI-mediated transfection of the pDNA/PEG–PLL polyplex micelles was carried out

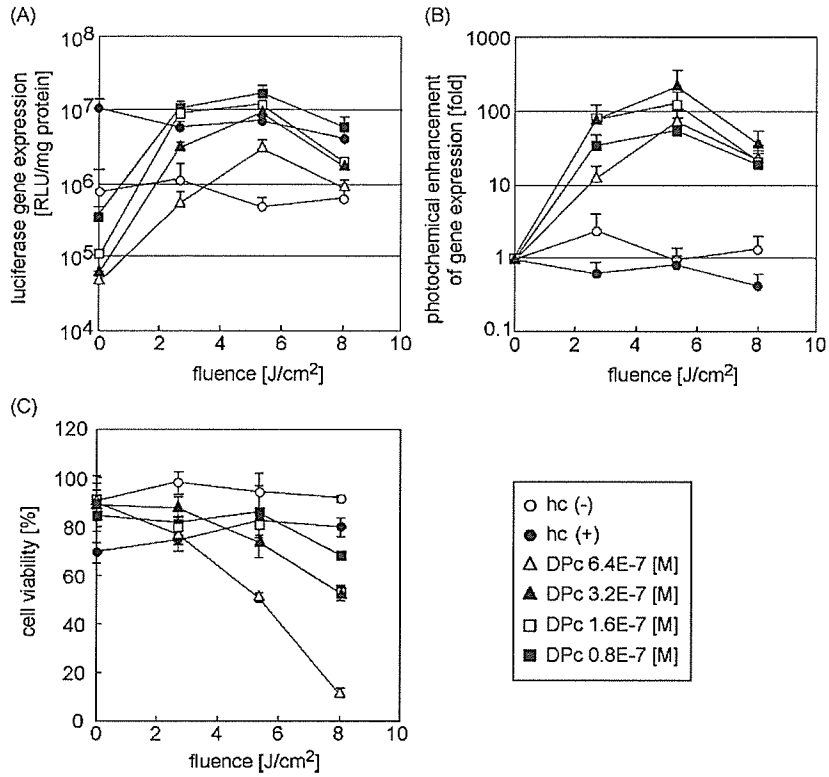


Figure 6. The effects on the DPc concentration and fluence on the transfection efficiency (A), photochemical enhancement of the gene expression (B) and photocytotoxicity (C) in the PCI-mediated transfection using the DPc-incorporated micelles. The light irradiation was performed 6 h after incubation with the pDNA- and DPc-incorporated micelles, followed by 48 h post-incubation in a fresh medium. The "hc" strands for hydroxychloroquine.

using DPc alone or $AlPcS_{2a}$, which was demonstrated to be an effective photosensitizer in the PCI (Høgset et al. 2002, 2004). These results are shown in Figures 7 and 8, respectively. Also, to easily compare the main differences between the results in Figures 6–8, the effects of each photosensitizer on the photochemical enhancement of the gene expression and cell viability at the fluence of 5.4 J/cm$^2$ are summarized in Table I. In the PCI using DPc alone, the highest transfection efficiency of the polyplex micelles was obtained with a 25–50% reduced cell viability (Figure 7(A) and (C)). The PCI using $AlPcS_{2a}$ showed a transfection activity comparable to that using the DPc-incorporated micelles; however, the photochemical enhancement of the transgene expression was accompanied by an inevitable photocytotoxicity (Figure 8(A) and (C)). Eventually, the PCI using the combination of the pDNA- and DPc-incorporated micelles showed the highest photochemical enhancement of the gene transfection of the polyplex micelles (Figure 6(B)), which may be attributed to the reduced transfection efficiency at comparatively high-concentrations of the DPc-incorporated micelles under non-irradiated conditions as discussed above as well as actual increases in the transfection efficiency. Such a high-light-selectivity of the gene transfection might be advantageous for accomplishing the site-directed gene transfer using the PCI concept. More importantly, the PCI using the DPc-incorporated micelles showed an appreciably wide range of safe DPc concentrations and light doses, in which a remarkable enhancement of the transfection was achieved without a substantial decrease in the cell viability (Figure 6(B) and (C)). The efficacy of this system was prominent even when compared with those of other systems using DPc alone and $AlPcS_{2a}$ as shown in Table I.

To achieve a systemic PCI-mediated gene delivery utilizing micellar nanocarriers, polymeric micelles are required to accumulate in the target tissues and be taken up by the target cells, of which processes are known to occur in a time-dependent manner. On the other hand, the timing of the photoirradiation may be a critical factor in the PCI-mediated transfection (Prasmickaite et al. 2001). Hence, the effect of the photoirradiation timing on the photochemical transfection was then investigated. First, the effect of the prolonged incubation before photoirradiation was examined: after a 24 h continuous incubation with the combination of the pDNA- and DPc-incorporated micelles, HeLa cells were subjected to the medium replacement, followed by photoirradiation at the fluence of 5.4 J/cm$^2$. The transfection efficacy was evaluated after a further 48 h of post-incubation. As seen in Figure 9, an approximately 50-fold photochemical enhancement in the gene expression while

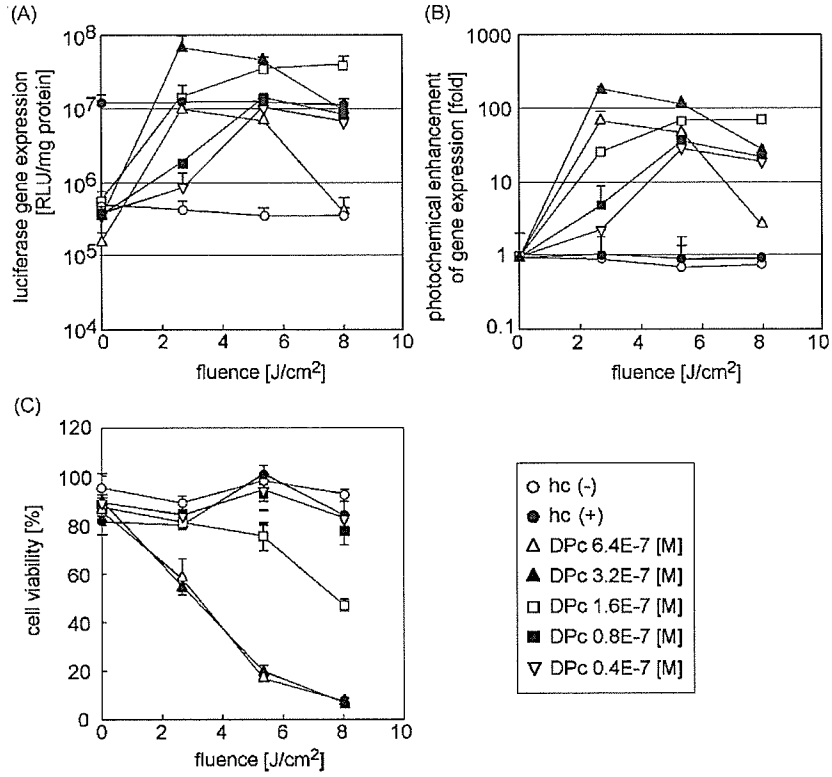


Figure 7. The effects on the DPc concentration and fluence on the transfection efficiency (A), photochemical enhancement of the gene expression (B) and photocytotoxicity (C) in the PCI-mediated transfection using DPc alone. The light irradiation was performed 6 h after incubation with the pDNA-incorporated micelles and free DPc, followed by 48 h post-incubation in a fresh medium.

maintaining more than an 80% cell viability was obtained under this condition, which appears to be consistent with Figure 5. Thus, the PCI using the DPc-incorporated micelles might be effective even after a prolonged incubation before photoirradiation. Note that the transfection efficiencies of the polyplex micelles under both irradiated and non-irradiated conditions decreased as the DPc concentration increased (Figure 9(A)), which may be due to the decreased cellular uptake of the polyplex micelles and/or interaction between the pDNA- and DPc-incorporated micelles as discussed above. In a second set of experiments, a certain lag time was placed before the photoirradiation of the HeLa cells in freshly replaced medium after a 6 h incubation with the combinational formulation of pDNA- and DPc-incorporated micelles. The transfection efficacy was evaluated 48 h after the photoirradiation (5.4 J/cm$^2$). As shown in Figure 10, post-incubation in the micelle-free medium after the 6 h treatment with the combinational micellar formulation resulted in a time-dependent decrease in the efficacy of the PCI-mediated transfection. This result seems to be consistent with the previous observation by Prasmickaite et al. (2001) suggesting that, in the PCI-mediated transfection, gene carriers may need to be translocated into the cytosol before their movement from the endosome to the lysosome. Therefore, to achieve a successful *in vivo* PCI-mediated gene delivery, the timing of the photoirradiation should be optimized in consideration of the balance between the effective accumulation of gene carriers as well as photosensitizers in the target cells and the prompt photo-induced translocation of gene carriers from the endosome to the cytosol before their movement to the lysosome.

The PCI is a smart concept, which can be basically used for the site-directed transfection in a light-inducible manner. In previous studies, $AlPcS_{2a}$ was demonstrated to be effective in the PCI (Høgset et al. 2002, 2004); however, the photochemical enhancement of the transfection was accompanied by the photocytotoxicity (Høgset et al. 2000). Although $AlPcS_{2a}$ is known to be internalized by the endocytic pathway, it is likely that $AlPcS_{2a}$ may interact with the plasma membrane to some extent as well as relocalize to some cytoplasmic organelles such as the mitochondria and endoplasmic reticulum during the photoirradiation, thereby inducing the inevitable photocytotoxicity (Moan et al. 1994; Macdonald and Dougherty 2001). Hence, considerable efforts have been devoted to the optimization of the experimental conditions for reducing the photocytotoxicity in the PCI-mediated transfection (Høgset et al. 2000). Also, the delivery of photosensitizers to the target cell should be taken into consideration in order to accomplish the *in vivo* PCI-mediated gene delivery.